

PROJECT COMPLETION REPORT

1. Title of the Project: Synthesis of mixed-ligand peroxo complexes of vanadium and tantalum and exploration of their biochemical properties
2. Principal Investigator : Dr. Gangutri Saikia
3. Mentor: Dr. Nashreen S. Islam
4. Implementing Institution and other collaborating Institution(s): Tezpur University
5. Date of Commencement: 15.05.2018
6. Planned Date of Completion: 15.05.2020
7. Actual Date of Completion: 15.10.2020
8. Objectives as stated in the project proposal:
 - I. To synthesize newer peroxo complexes of vanadium and tantalum by employing ligands such as amino acids, peptides and water soluble functionalized polymer both synthetic as well as natural biopolymer.
 - II. To comprehensively characterize the synthesized compounds by using physico-chemical and spectral techniques.
 - III. To determine the nature and hydrolytic stability of the newly synthesized compounds in solid state as well as in solution.
 - IV. To investigate the biochemical properties of the synthesized compounds with various enzyme systems such as calcineurin-a serine/ threonine phosphatase, alkaline phosphatase(ALP), acid phosphatase (ACP), catalase, protein tyrosine phosphatase (PTP) and superoxide dismutase (SOD).
9. Deviation made from original objectives if any, while implementing the project and reasons thereof:

We have also investigated the catalytic activities of polymer supported peroxidovanadium complexes. The reason for this deviation-

1. Due to the insolubility of the biopolymer supported peroxidovanadium complex (ChpV) in aqueous solution, we could not be able to do the biochemical study of this complex. Therefore, it was decided to carry out catalytic activity study of the complex in organic oxidation.
 2. To compare the catalytic activity of the heterogeneous peroxidovanadium complex (ChpV) with homogeneous one, catalytic activity of water soluble polymer supported peroxidovanadium complex (PAmV) was explored.
- 10.** Experimental work giving full details of experimental set up, methods adopted, data collected supported by necessary table, charts, diagrams & photographs:

Annexure I

- 11.** Detailed analysis of results indicating contributions made towards increasing the state of knowledge in the subject:

Annexure II

- 12.** Conclusions summarising the achievements and indication of scope for future work:

In this project, we have introduced a set of peroxovanadium and peroxotantalum complexes immobilized on non-cross linked and linear polymer matrices. The spectral analysis data provided satisfactory evidences for the mode of co-ordination of the pendant ligands to the V(V) and Ta(V) centre, and composition of the macro complexes. The peroxovanadium (V) compound immobilized on chitosan displayed efficiency as cost-effective environmentally safe heterogeneous catalyst for the selective oxidation of sulfides to their respective sulfoxides in aqueous medium. In comparison to the heterogeneous catalyst, soluble polymer supported pV complex showed less selectivity in aqueous medium though in organic medium, it demonstrated high performance, selectivity and recyclability, as well. We have carried out a comparative study on the biological activity of the newly synthesized tantalum (V) peroxides in comparison to vanadium (V) peroxides in similar macroligand environment by using wheat thylakoid acid phosphatase as model enzyme. The anchored pTa compounds, like their pV analogues, remain hydrolytically stable in a wide range of pH values including at acidic pH. Most importantly, the pTa compounds displayed extraordinary stability in the presence of catalase, by partially retaining the co-ordinated peroxido groups even beyond 4 h of incubation with the enzyme. In contrast, complete loss of peroxido groups from peroxidovanadate compounds occurred under catalase action within ca. 30 min of incubation. Furthermore, our experiments establish that, although the tested complexes of both Ta(V) and V(V) exert strong inhibitory effects on ACP, the pTa derivatives showed greater efficiency, at nearly a 2–3 fold lesser dose, than the corresponding pV compounds. Detailed enzyme kinetic analysis results demonstrated that the pV and pTa compounds exhibit a distinct mechanistic preference to inhibit the enzyme function via a noncompetitive pathway. Thus, it may be expected that our findings will provide a facile route to the design of potent peroxidometallate based

inhibitor systems which may serve as selective probes of non-competitive sites of phosphatases.

13. New Observations: In this study, it has been observed for the first time that peroxidotantalum derivatives are 2-3 fold more active as inhibitors of wheat thylakoid acid phosphatase enzyme compared to their V containing analogues.

14. Innovations:

15. Application Potential:

a. Immediate:

b. Long Term: It can be expected that our findings will provide a facile route to the design of potent peroxidometallate based inhibitor systems which may serve as selective probes of non-competitive sites of phosphatases.

16. S&T benefits accrued:

a. List of Research publications

S No	Authors	Title of paper	Name of the Journal	Volume	Pages	Year
1	Gangutri Saikia, Kabirun Ahmed, Sandhya Rani Gogoi, Mitu Sharma, Hiya Talukdar, Nashreen S. Islam	A chitosan supported peroxidovanadium (V) complex: Synthesis, characterization and application as an eco-compatible heterogeneous catalyst for selective sulfoxidation in water	Polyhedron	159	192-205	2019
2	Gangutri Saikia*, Hiya Talukdar, Kabirun Ahmed, Nand Kishore Gour and Nashreen S. Islam*	Tantalum(V) peroxido complexes as phosphatase inhibitors: a comparative study vis-a-vis peroxidovanadates	New Journal of Chemistry	45	12842-12862	2021

b. Manpower trained on the project

i) Ph.D. produced: I, Gangutri Saikia, P.I. of the project acquired Ph.D. degree during project period, in 2020.

ii) Other Technical Personnel trained

c. Patents taken, if any

17. Financial Position:

S No	Financial Position/ Budget Head	Funds Sanctioned	Expenditure	% of Total cost
1.	Salaries/ Manpower costs	3,60,000/-	6,76,452/-	100%
2.	Equipment	2,50,000/-	2,48,786/-	99%
3.	Supplies & Materials	2,00,000/-	2,17,404/-	100%
4.	Contingencies	15,000/-	21,400/-	100%
5.	Travel	15,000/-	11,797/-	79%
6.	Overhead Expenses	82,500/-	1,18,914/-	100%
7.	Others, if any	3,75,478/-	1,981/-	100%
	Total	12,97,978/-	12,96,734/-	100%

18. Procurement/ Usage of Equipment

a)

S No	Name of Equipment	Make/ Model	Cost (FE/ Rs) (Without Tax)	Date of Installation	Utilisation Rate (%)	Remarks regarding maintenance/ breakdown
1	Magnetic stirrer with hot plate	Remi & 2MLH	18,810/-	4.02.2019	100	
2	Micropipette	Genexy & Nichipet EXII	21,390/-	4.02.2019	97	
3	Premium pipette	Abdos	12,900/-	4.02.2019	97	
4	Ultra sonic cleaner with basket	Riviera	16,099/-	4.02.2019	82	
5	pH spear tester	Thermo scientific - Eutech, Riviera	23,800/-	4.02.2019	89	
6	Autoclave ST – Standard,	Equitron, Model:74 07ST	24,200/-	4.02.2019	80	

7	Millipore Vacuum pump	Merck	25,000/-	4.02.2019	90	
8	Heating mantle	JSGW	2,059/-	4.02.2019	90	
9	Digital stirring hot plate	Corning Model: PC420D	28,500/-	4.02.2019	95	
10	Laptop	Dell	39,490/-	4.03.2019	98	
11	Canon laserjet printer 6030	Canon	9,900/-	4.03.2019	75	
12	Refrigerator	LG, GLB201 ARGX	18,000/-	6.03.2019	100	

b) Plans for utilising the equipment facilities in future

The equipments will be utilized fully in future by the host institution.

Name and Signature with Date

a. Grangotri Saitia 23/11/22
(Principal Investigator)

b. N. S. Galam
(Mentor)

ANNEXURE I

1. Synthesis of the peroxidometallate macrocomplexes

1.1 Synthesis of $[\text{VO}(\text{O}_2)_2(\text{NH}_2)]$ -chitosan (ChpV)

The procedure is as follows- V_2O_5 (0.56 g) was dissolved in 30% H_2O_2 (10 mL) maintaining temperature below 4 °C. The initial pH of the resulting clear yellow solution was found to be *ca.* 1. The pH of the solution was raised up to *ca.* 7 by adding concentrated potassium hydroxide (*ca.* 8 M) dropwise with constant stirring. Keeping the reaction mixture stirred in an ice-bath, 1 g of chitosan was added to it. The resulting reaction mixture was allowed to stand for 24 h under constant stirring, maintaining the temperature below 4 °C. Subsequently, the supernatant liquid was decanted and the resulting yellowish residue was washed repeatedly with acetone.

1.2 Synthesis of $[\text{V}_2\text{O}_2(\text{O}_2)_4(\text{amide})]$ -PAm [PAm=poly(acrylamide)] (PAmV)

The synthesis of poly(acrylamide) supported peroxidovanadium complex was achieved by reacting vanadium pentoxide (V_2O_5) (1.28 g) with the polymer poly(acrylamide) (PAm) (1 g) dissolved in minimum volume of water in presence of 30% H_2O_2 (12 mL). Hydrogen peroxide was added to the reaction mixture with constant stirring while maintaining the temperature below 4°C in an ice bath until a clear solution was obtained. At this stage, the pH of the solution was found to be *ca.* 2. Then 8 N NaOH solution was added dropwise with constant stirring to raise the pH to *ca.* 6. The reaction mixture was allowed to stand for 3 h. After completion of that period, pre-cooled acetone was added to it under vigorous stirring. A light yellow colored sticky compound separated out from the reaction mixture which turned into microcrystalline solid upon repeated treatment with acetone. The product was isolated by centrifugation and washed with cold acetone.

1.3 Synthesis of $[\text{Ta}(\text{O}_2)_3(\text{carboxylate})]$ -PA, [PA= poly(sodium acrylate)] (PATa)

The reaction procedure developed for the synthesis of PATa consisted of gradual addition of 10 mL 30% H_2O_2 , to a mixture of the precursor complex sodium tetraperoxidotantalate $\text{Na}_3[\text{Ta}(\text{O}_2)_4]\cdot\text{H}_2\text{O}$ (1.4 g) with 1 g of the polymer, PA dissolved in minimum volume of water. The pH of the reaction solution was recorded to be *ca.* 7.0. Dilute HNO_3 (4 M) was added dropwise to the system until the pH was lowered to *ca.* 6.0. The reaction mixture was allowed to stand for about 3 h in an ice-bath. The temperature was maintained below 4 °C throughout the procedure. Then, pre-cooled acetone was added to it to induce precipitation under continuous stirring. The supernatant liquid was decanted off and the residue was treated repeatedly with acetone to obtain the desired microcrystalline product which was separated by centrifugation.

1.4 Synthesis of $[\text{Ta}(\text{O}_2)_3(\text{sulfonate})_2]$ -PSS, PSS= poly(sodium 4-styrene sulfonate) (PSSTa)

The methodology for the synthesis of PSSTa is as follows- sodium tetraperoxidotantalate $\text{Na}_3[\text{Ta}(\text{O}_2)_4]\cdot\text{H}_2\text{O}$ (0.22 g) was solubilized in 4 mL of 30 % H_2O_2 in presence of the polymer,

PSS (2 mL). The pH of the reaction solution was found to be *ca.* 5.8 which was adjusted to *ca.* 6.0 by the addition of NaOH. The system was allowed to stand while maintaining the temperature below 4 °C. Pre-cooled acetone was added under vigorous stirring to induce precipitation. Similarly as mentioned in the synthesis of **PATa**, the supernatant liquid was decanted off and the residue was washed repeatedly with acetone to obtain the microcrystalline product.

2. Elemental analysis method

The vanadium and tantalum content of the synthesized compounds were determined by atomic absorption spectroscopy (AAS) employing Thermo iCE 3000 series atomic absorption spectrophotometer (model analyst 200) and inductively coupled plasma optical emission spectrophotometer (ICP-OES) (Perkin Elmer, OPTIMA 2100 DV). The vanadium content was also determined volumetrically by iodometric method described in earlier paper [1]. The counter ion, sodium or potassium content was measured by ICP-OES. Elemental analysis for C, H and N was carried out on an elemental analyzer (Perkin-Elmer 2400 series II). The peroxide content of the compounds was determined by the procedure reported previously [2].

3. Physical and spectroscopic measurements

The IR spectra were recorded by making pressed pellets of samples with KBr using Perkin-Elmer spectrum 100 FTIR spectrophotometer. Raman spectrum of the compound was recorded using a Renishaw InVia Raman microscope equipped with an argon ion laser with an excitation wavelength of 514 nm and a laser maximum output power of 20 mW. The diffuse reflectance electron absorption spectra were measured by using a Hitachi U-3400 spectrophotometer equipped with a diffuse reflectance accessory with an integrating sphere of 60 mm inner diameter using BaSO₄ as the standard. The powder X-ray diffraction (XRD) patterns were recorded on a Rigaku X-ray diffractometer (Miniflex, UK) using Cu K α ($\lambda = 0.154$ nm) radiation at a scanning rate of 10°C min⁻¹ in the 2 θ range 10–70°. XPS measurements were carried out by using Thermo Fisher Scientific Instrument's X-ray photo spectrometer equipped with Al K α (monochromatic) X-ray source. The source was operated at 12 kV. The base pressure was maintained at 2 X 10⁻⁹ mbar in the analyzing chamber. Charging of the samples was corrected by setting the binding energy of the adventitious carbon (C 1s) at 284.6 eV. Thermogravimetric analysis (TGA) was carried out on a SHIMADZU TGA-50 system at a heating rate of 10 °C min⁻¹ under N₂ atmosphere using an aluminium pan. Scanning electron microscopy (SEM) and Energy-dispersive X-ray analysis of the compound were obtained using a JEOL JSM-6390LV scanning electron micrograph attached with an energy-dispersive X-ray detector. Scanning was done in the 1–20 μ M range, and images were taken at a magnification of 15–20 kV. Data were obtained using INCA software. Standardization of the data analysis is an integral part of the SEM-EDX instrument employed. The ¹³C NMR spectra for chitosan and ChpV were recorded using a JEOL JNM-ECX400II spectrometer at a carbon frequency of 100.5 MHz, 1024 X-resolution points, number of scans 1300, 29 ms of acquisition time, and 5 s of relaxation delay. For all the water soluble complexes, the ¹³C NMR spectra were recorded with JEOL JNM-ECS

400 spectrometer at a carbon frequency of 100.5 MHz, 32768 X-resolution points, number of scans 8000-20000, 1.04 s acquisition time and 2.0 s relaxation delay with the ^1H NMR decoupling method in D_2O as solvent. The NMR spectra of organic sulfoxides and sulfones were recorded in CDCl_3 . ^{51}V NMR spectra were recorded on a JEOL JNM-ECS400 spectrometer at a vanadium frequency of 105.154 MHz with the samples in a 10 mm spinning tube using a sealed co-axial tube containing D_2O , which provided the lock signal. The chemical shift data were recorded as negative values of ppm (δ) in the low-frequency direction with reference to VOCl_3 at 293 K. The surface areas were determined by nitrogen adsorption/desorption measurements based on the Brunauer-Emmett-Teller (BET) method at 77.3 K on a standard module NOVA 1000E, Quantachrome Instrument. The pore size and pore volumes were measured by the Barrett-Joyner-Halenda (BJH) model in the same Quantachrome Instrument. Magnetic susceptibilities of the complex was measured by the Gouy method, using $\text{Hg}[\text{Co}(\text{NCS})]$ as the calibrant. The Melting points of the products were determined in open capillary tubes on a Büchi Melting Point B-540. The GC analysis was done using a CIC model 2010 gas chromatograph and an SE-52 packed column (length 2 m, 1/8 inch OD) with a flame ionization detector (FID) and nitrogen as the carrier gas (30 mL min^{-1}).

4. Catalytic activity study:

4.1 General procedure for selective oxidation of sulfides to sulfoxides

In the representative procedure for selective oxidation of sulfides to sulfoxides, organic substrate MPS (5 mmol) was added to the reaction mixture consisting of catalyst **ChpV** (21.00 mg, containing 0.005 mmol of V) in 5 mL of H_2O . This was followed by the addition of 30% H_2O_2 (2.82 mL, 25 mmol) to the reaction system contained in a round bottom flask. The molar ratio of V:substrate and that of substrate: H_2O_2 was maintained at 1:1000 and 1:5, respectively. For the reaction conducted in acetonitrile, V:substrate and the substrate: H_2O_2 were adjusted at 1:1000 and 1:2 keeping rest of the reaction conditions identical to the reaction conducted in water. The reaction was conducted at ambient temperature under continuous magnetic stirring.

In the procedure for selective sulfoxidation with water soluble peroxidovanadium complex, **PAmV** as catalyst, the organic substrate (5 mmol) was added to a mixture of catalyst (containing 0.005 mmol of V), **PAmV** (1.6 mg) and methanol (5 mL), maintaining a molar ratio of V:MPS::1:1000 at room temperature under continuous magnetic stirring. 30% H_2O_2 (10 mmol) was added afterwards keeping the molar ratio of substrate: H_2O_2 as 1:2 for the reaction.

The progress of the reaction was monitored by thin layer chromatography (TLC) and GC. In case of heterogeneous catalyst, **ChpV**, the used catalysts were recovered by filtration and washed with acetone for further use. The extraction procedure of the product and the unreacted substrates was comprised of addition of diethyl ether to the reaction mixture after completion of the reaction. In case of homogeneous catalyst, **PAmV**, the aqueous portion of the reaction mixture contained the catalyst after removal of the organic part and was reused for another batch of reaction with fresh addition of MPS (5 mmol), 30 % H_2O_2 (10 mmol), and solvent MeOH (5

mL). The extracted products were dried over anhydrous Na_2SO_4 and distilled under pressure to remove the excess solvent.

5. Investigation of biochemical properties of the peroxidometal complexes

5.1 Stability of the pTa compounds in aqueous solution

To determine the stability of the compounds in solution, a stock solution of 0.2 mM concentration (100 mL) was prepared for each of the compounds by dissolving a weighed amount of the respective compounds **TpTa** (0.079 mg/mL), **PATa** (0.123 mg/mL) and **PSSTa** (0.235 mg/mL) in water. The peroxide content in aliquots drawn from the stock solution was determined at different time intervals for a period of 12 h by peroxide estimation method. Stability of the compounds was measured similarly at different pH values- pH 4.6, pH 7.0 and pH 8.0 maintained by using phosphate buffer (50 mM), pH 1.2 and pH 2.1 (50 mM KCl/HCl buffer), and pH 3.1 (50 mM citrate buffer). Moreover, ^{13}C NMR spectra of the compounds were monitored over a period of 12 h for any possible change. For the polymer anchored pTa compounds, the compounds concentrations were calculated on the basis of actual peroxidotantalum loading (mmol g^{-1}).

5.2 Method of acid phosphatase activity measurement

The activity of acid phosphatase was measured spectrophotometrically by using p-nitrophenyl phosphate (p-NPP) as substrate [3]. In the standard protocol, the reaction mixture contained enzyme ($18.38 \mu\text{g protein mL}^{-1}$) and different concentrations of the inhibitor species [concentration varies between 5-50 μM for **DPV**, 5-25 μM for **PAV** and **PATa**, 0.5-2.5 μM for **TpTa** and **PSSV**, and 0.2-1.0 μM for **PSSTa** in acetate buffer (0.1 M, pH= 4.6) as shown in **Fig. 26**. For the polymer anchored complexes, concentrations were calculated on the basis of metal loading (mmol g^{-1}). The reaction was started by the addition of p-NPP to the reaction mixture which was pre-incubated for 5 min at 30 °C. After 30 min of incubation, the reaction was terminated by adding 0.9 mL of 0.5 M NaOH solution. The release of p-nitrophenol from the substrate was determined by measuring the absorbance of the reaction solution at 405 nm (molar extinction co-efficient of p-nitrophenolate = $18000 \text{ M}^{-1} \text{ cm}^{-1}$) [4]. The enzyme activity in absence of the inhibitors was used as control. The half-maximal inhibitory concentration (IC_{50}) values were determined graphically giving 50% inhibition of the enzyme. All the experiments were performed in triplicate. The data in the figures were presented as the average \pm SE from the three separate experiments.

5.3 Determination of kinetic parameters

The kinetic studies were carried out by using substrate concentration in the range of 50-300 μM in presence or absence of each of the inhibitor species with varied concentrations as shown in **Fig. 28** and **Fig. 29**. The kinetic constants, maximum velocity (V_{max}) and Michaelis constant (K_m) were determined from Lineweaver-Burk plots by rearranging Michaelis-Menten equation [3d,5].

$$\frac{1}{V} = \frac{K_m}{V_{max}[S]} + \frac{1}{V_{max}} \quad \text{.....1}$$

In the present case, the expression (2) was used to determine rate of the reaction

$$V = \left\{ \frac{V_{max} \times [S]}{K_m \left(\frac{1 + [I]}{K_i} \right) + [S] \left(\frac{1 + [I]}{K_{ii}} \right)} \right\} \quad \text{.....2}$$

Where V is the velocity, [S] is p-NPP concentration and [I] refers to the inhibitor concentration. K_i and K_{ii} are the inhibitory constants for the competitive and non-competitive part, respectively. They were determined from the secondary plots of initial rate data by linear regression analysis. K_i value was obtained from the x-intercepts of the re-plots where the slopes from the L-B plots were plotted against inhibitor concentrations. K_{ii} value was also determined from x-intercepts of the plots of intercepts that were obtained from Lineweaver plots against inhibitor concentrations.

6. DATA COLLECTED:

6.1 CHARACTERIZATION OF NEWLY SYNTHESIZED COMPLEXES:

6.1.1 Elemental Analysis

Table 1 Elemental analysis of the compounds **ChpV**, **PAmV**, **PATa** and **PSSTa**

Compound	% found from elemental analysis (% Obtained from EDX spectra)									M:O ₂ ²⁻	Metal loading ^b (mmolg ⁻¹)
	C	H	N	O	Na	K	S	M	O ₂ ²⁻		
ChpV	28.97 (28.78)	5.55	6.46 (6.32)	43.30 (43.30)		9.39 ^a (9.67)		11.67 ^a (11.90)	14.98	1:2	2.34
PAmV	22.3 (22.9)	2.9	8.9 (8.7)	45.2 (45.2)	8.0 (7.6)			15.9 ^a (15.6)	19.5	1:2	3.06
PATa	18.2 (21.2)	1.7		35.3 (35.3)	14.9 (14.1)			31.2 ^a (29.3)	15.7	1:3	1.62
PSSTa	33.5 (32.8)	2.6		28.3 (28.3)	12.0 (12.2)		12.1 (12.1)	15.3 ^a (14.6)	8.1	1:3	0.85

M= V or Ta. ^aObtained from ICP-OES.

$${}^b\text{Metal loading} = \frac{\text{Observed metal \% X 10}}{\text{Atomic weight of metal}}$$

6.1.2 SEM-EDX Analysis

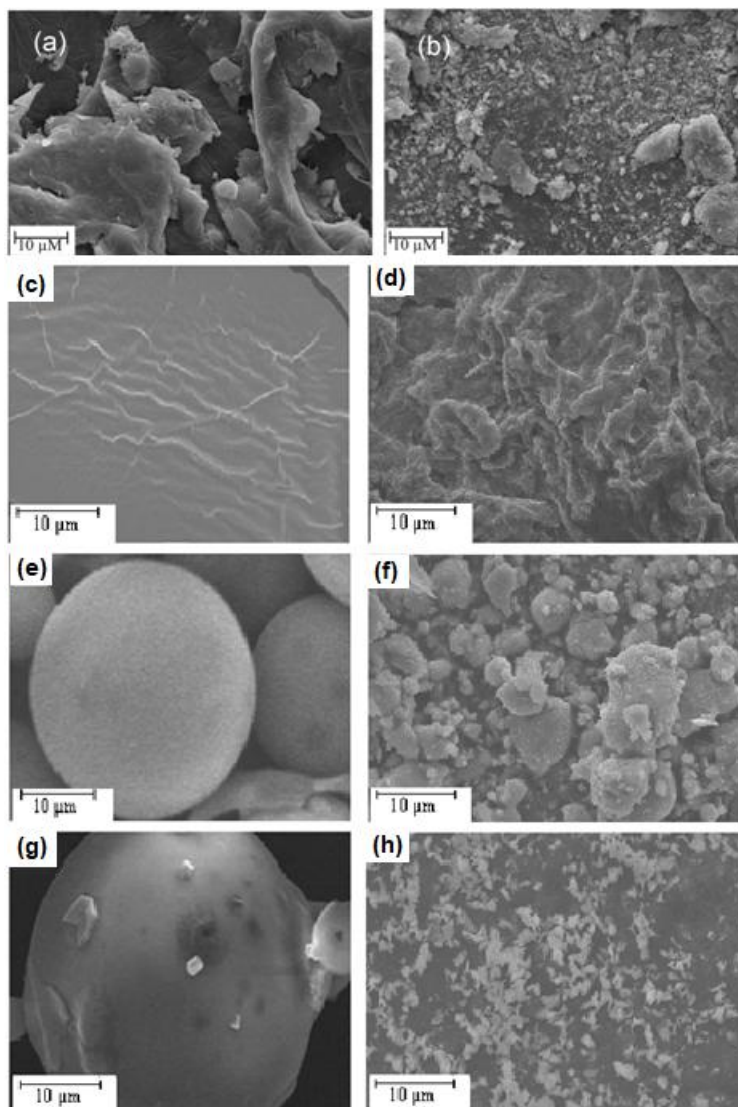


Fig. 1 Scanning electron micrographs of (a) chitosan, (b) **ChpV**, (c) PAm, (d) **PAmV**, (e) PA, (f) **PATa**, (g) PSS, and (h) **PSSTa**

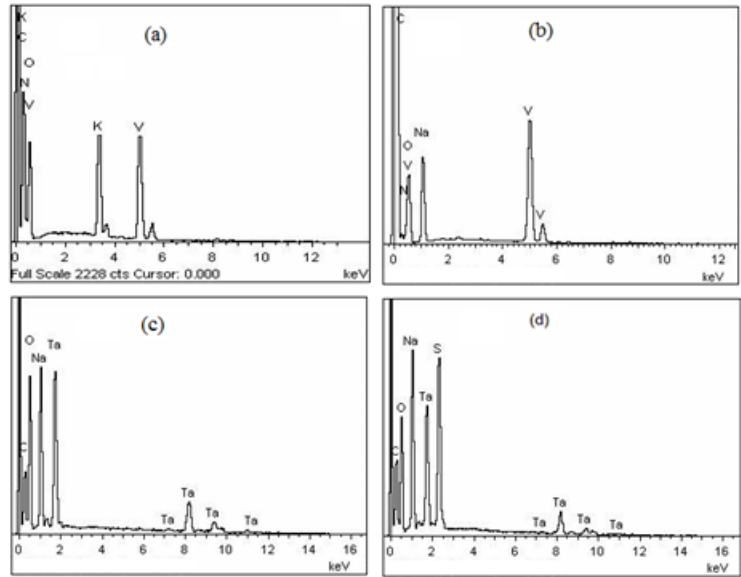


Fig. 2 EDX spectra of (a) **ChpV**, (b) **PAmV**, (c) **PATa**, and (d) **PSSTa**

6.1.3 X-ray diffraction studies

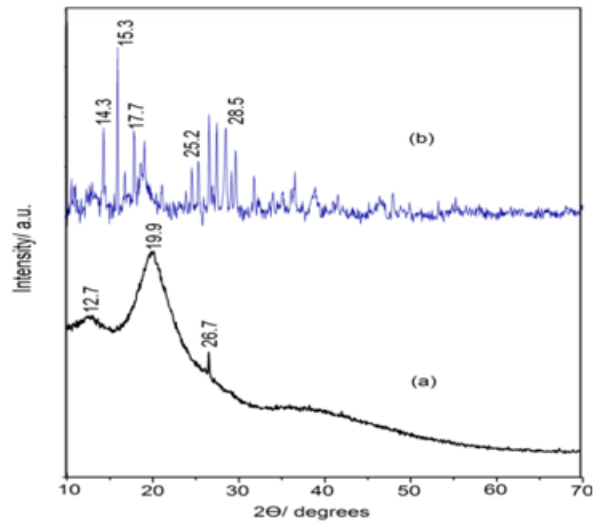


Fig. 3 X-ray diffraction (XRD) pattern of (a) chitosan, and (b) **ChpV**

6.1.4 X-ray photoelectron spectroscopy

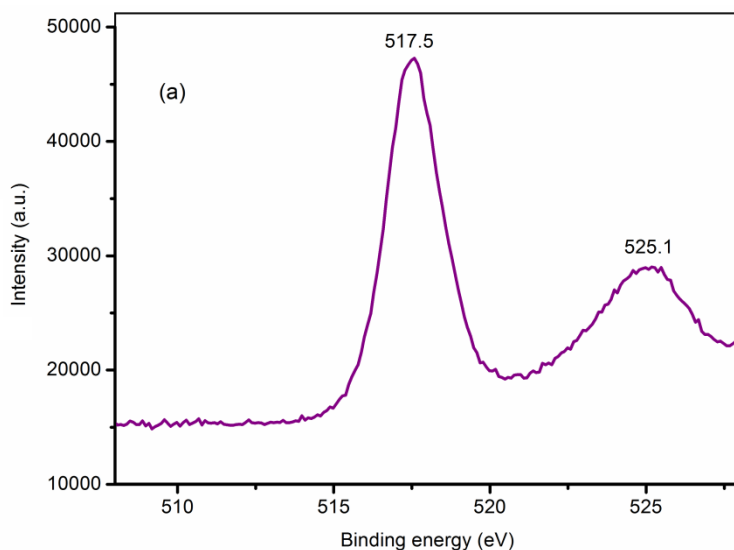


Fig. 4 XPS spectra of (a) V ($2p_{3/2}$), V ($2p_{1/2}$) peaks for **ChpV**

6.1.5 BET analysis

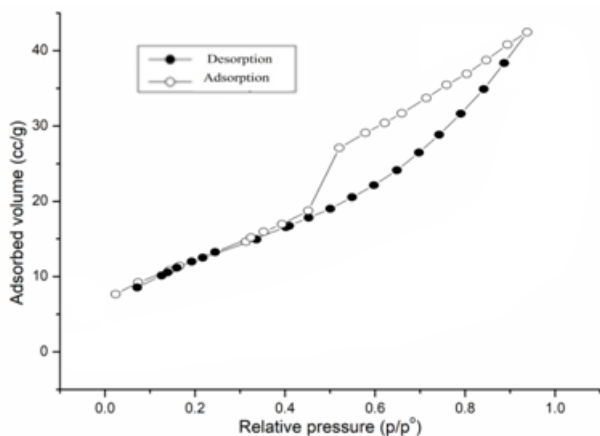


Fig. 5 Adsorption/desorption isotherm of **ChpV**

Table 2 BET surface area, V_{tot} and the pore radius of the polymer support, chitosan and polymer bound peroxidometal complexes

Compound	$S_{\text{BET}}^{\text{a}}$ (m^2/g)	$V_{\text{tot}}^{\text{b}}$ (mL/g)	Pore diameter (\AA)
Chitosan	3.0	0.05	32.0
ChpV	43.6	0.06	38.7

^aBET surface area. ^bTotal pore volume.

6.1.6 IR and Raman spectral studies

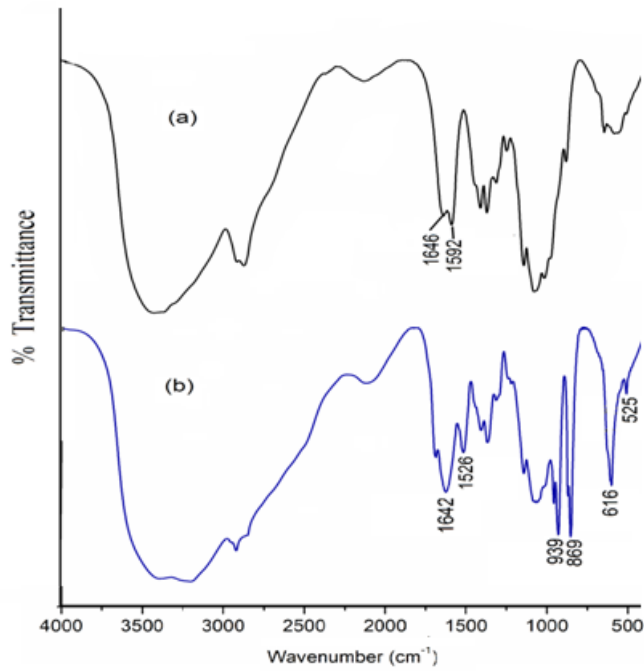


Fig. 6 IR spectra of (a) chitosan, (b) **ChpV**

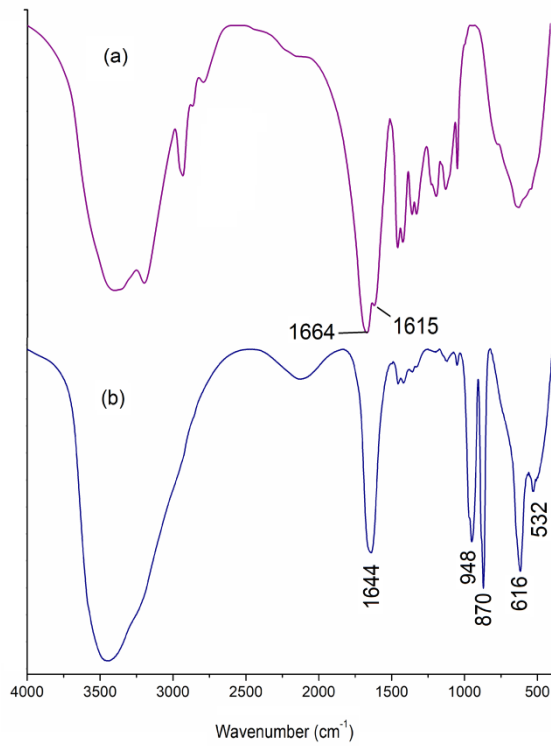


Fig. 7 IR spectra of (a) PAm and (b) **PAmV**

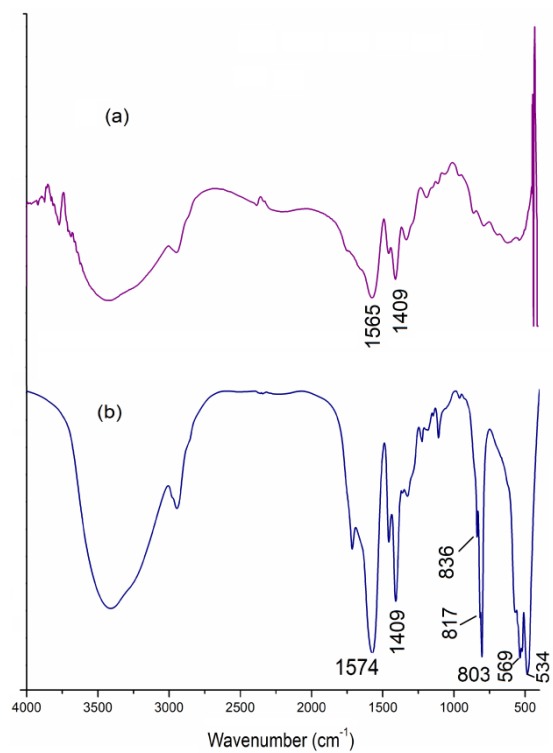


Fig. 8 IR spectra of (a) PA and (b) PATa

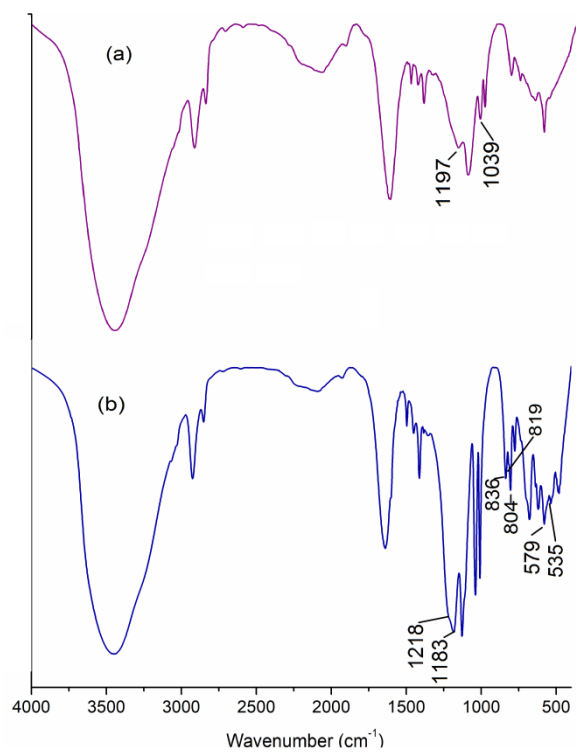


Fig. 9 IR spectra of (a) PSS and (b) PSSTa

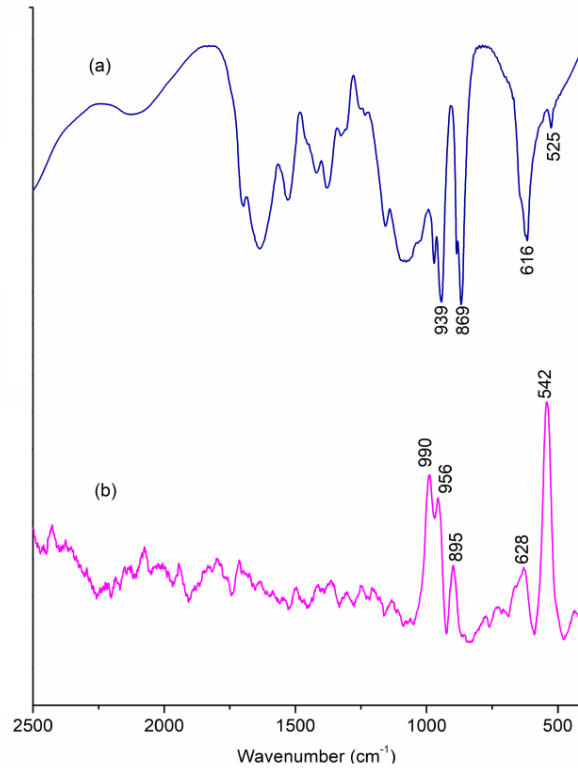


Fig. 10 (a) IR and (b) Raman spectra of **ChpV**.

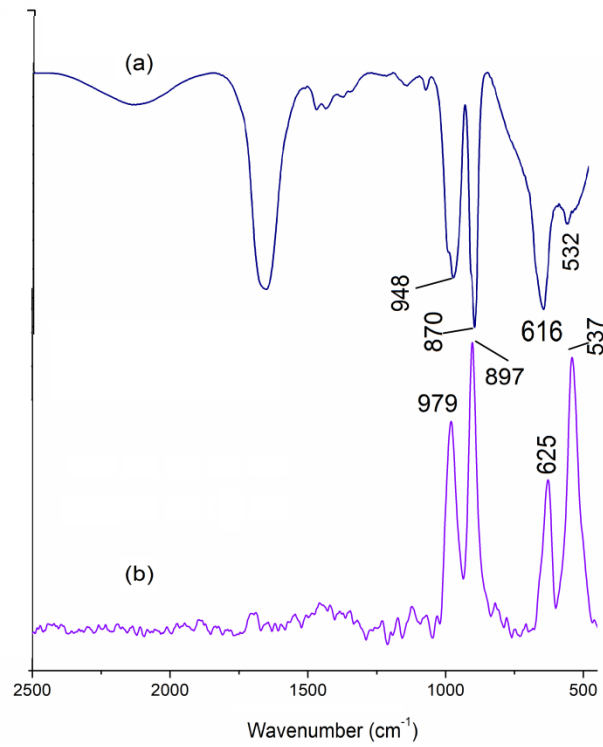


Fig. 11 (a) IR and (b) Raman spectra of **PAmV**

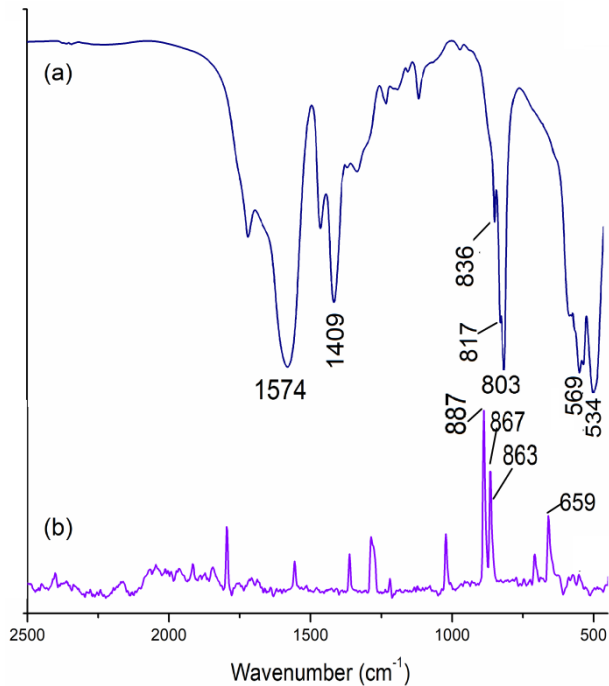


Fig. 12 (a) IR and (b) Raman spectra of **PATa**.

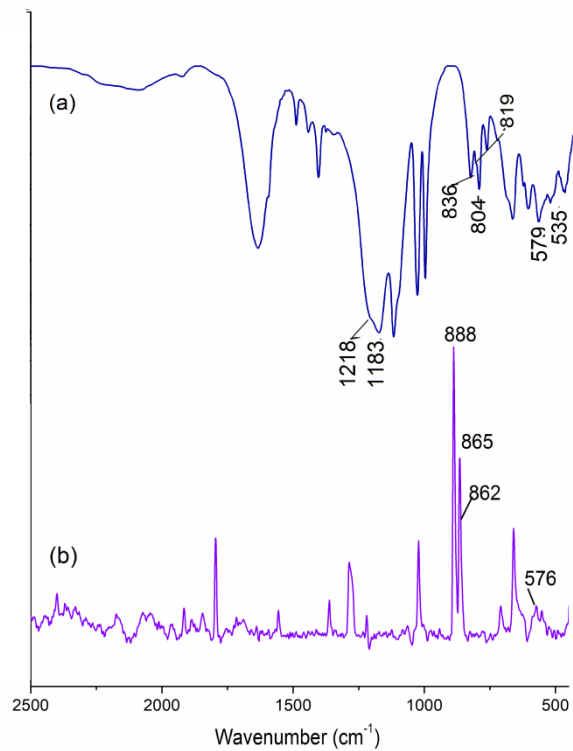


Fig. 13 (a) IR and (b) Raman spectra of **PSSTa**

Table 3 IR and Raman spectral data for the compounds **ChpV**, **PAmV**, **PATa** and **PSSTa**

Assignment		ChpV(cm ⁻¹)	PAmV(cm ⁻¹)	PATa (cm ⁻¹)	PSSTa (cm ⁻¹)
ν(O-O)	IR	869(s)	870(s)	836(sh), 817(sh), 803(s)	836(m), 819(sh), 804(m)
	R	895(m)	897(s)	887(s), 867(s), 863(sh)	888(s), 865(s), 862(sh)
ν _{as} (M-O ₂)	IR	616(s)	616(s)	569(sh)	579(m)
	R	628(m)	625(s)	659(m)	576(vw)
ν _s (M-O ₂)	IR	525(sh)	532(m)	534(s)	535(sh)
	R	542(s)	537(s)	441(s)	437(s)
ν(M=O)	IR	939(s)	948(s)		
	R	956(s)	979(s)		
ν(CO)	IR		1644(s)		
	R		1679(m)		
ν _{as} (COO)	IR			1574(s)	
	R			1554(m)	
ν _s (COO)	IR			1409(m)	
	R			1368(m)	
ν _{as} (S-O)	IR				1218(sh), 1183(s)
	R				1283(m), 1221(vw)
Amide I [ν (CO) + δ(NH)]	IR	1641(s)			
δ(NH)	IR	1561(sh)			
δ(O-H)	IR	1409(sh)			

^as, strong; m, medium; vw, very weak; sh, shoulder

6.1.7 Electronic spectral studies

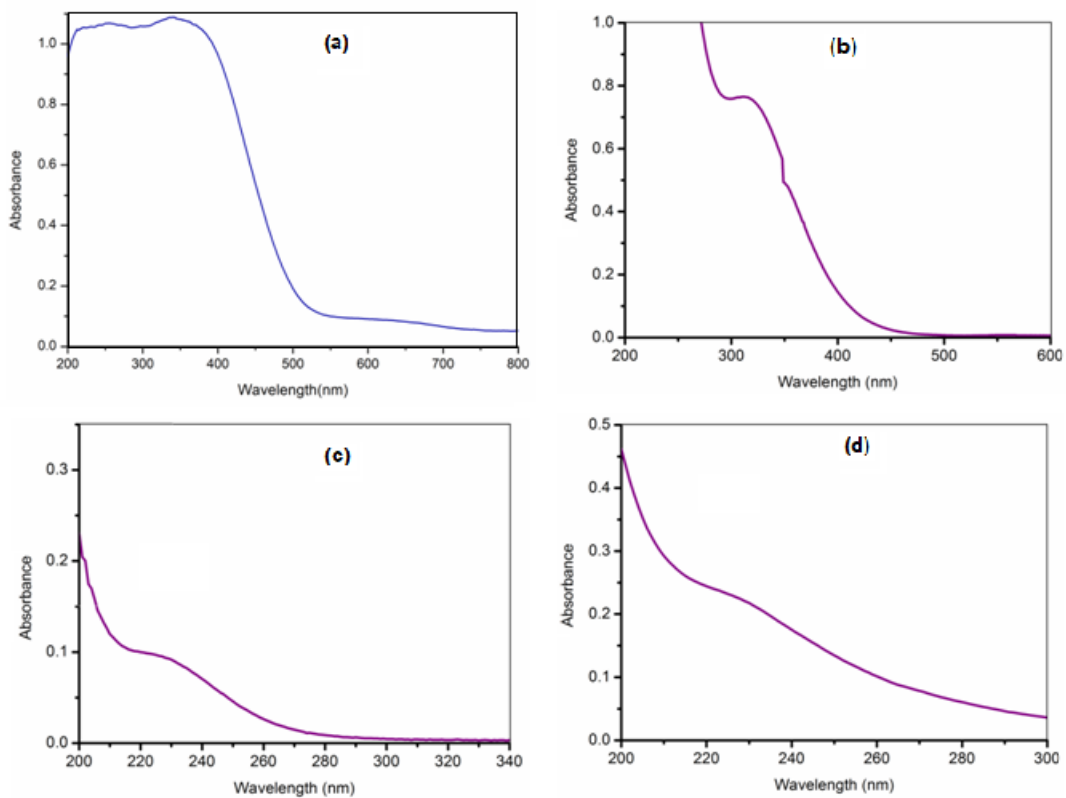


Fig. 14 (a) Solid state electronic spectrum of **ChpV**, solution state UV-visible spectra of (b) **PAmV**, (c) **PATa**, and (d) **PSSTa**

6.1.8 ^{13}C NMR studies

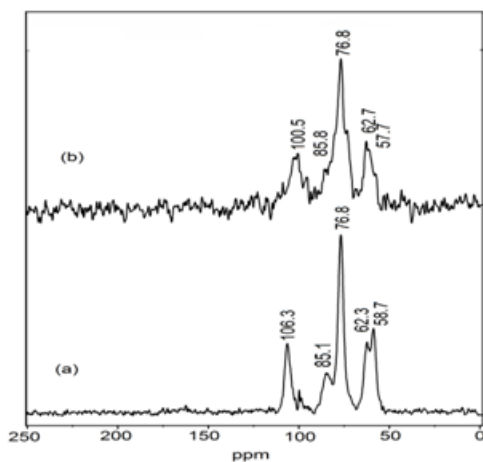


Fig. 15 ^{13}C NMR spectra of (a) chitosan, and (b) **ChpV**

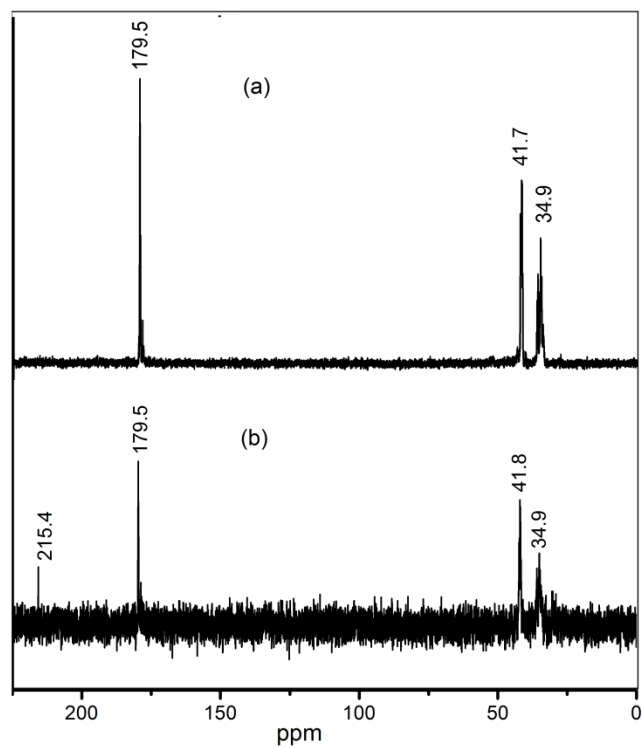


Fig. 16 ^{13}C NMR spectra of (a) PAm and (b) PAmV in D_2O .

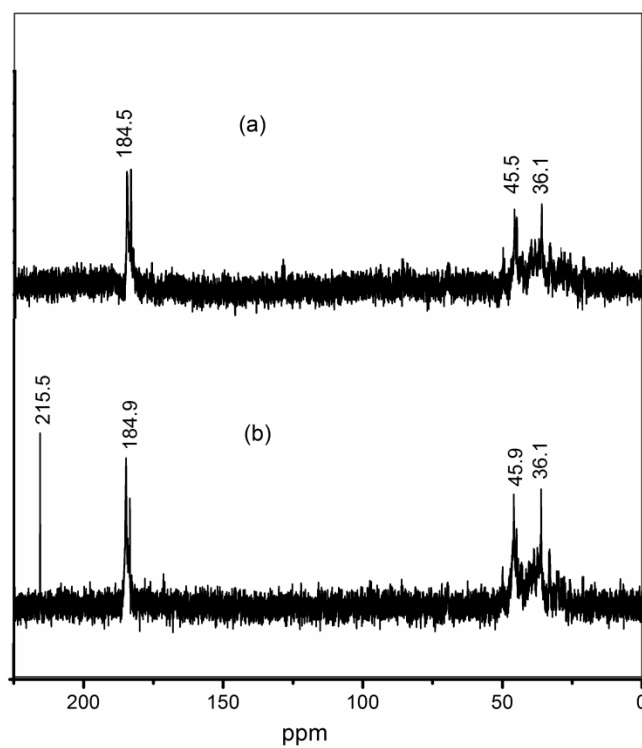


Fig. 17 ^{13}C NMR spectra of (a) PA and (b) PATa in D_2O .

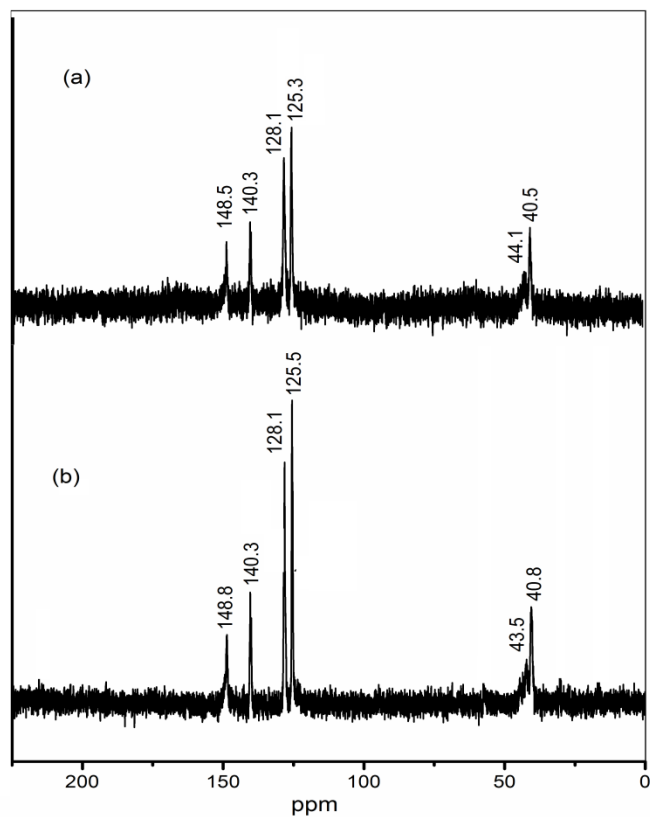


Fig. 18 ^{13}C NMR spectra of (a) PSS and (b) PSSTa in D_2O .

6.1.9 ^{51}V NMR studies

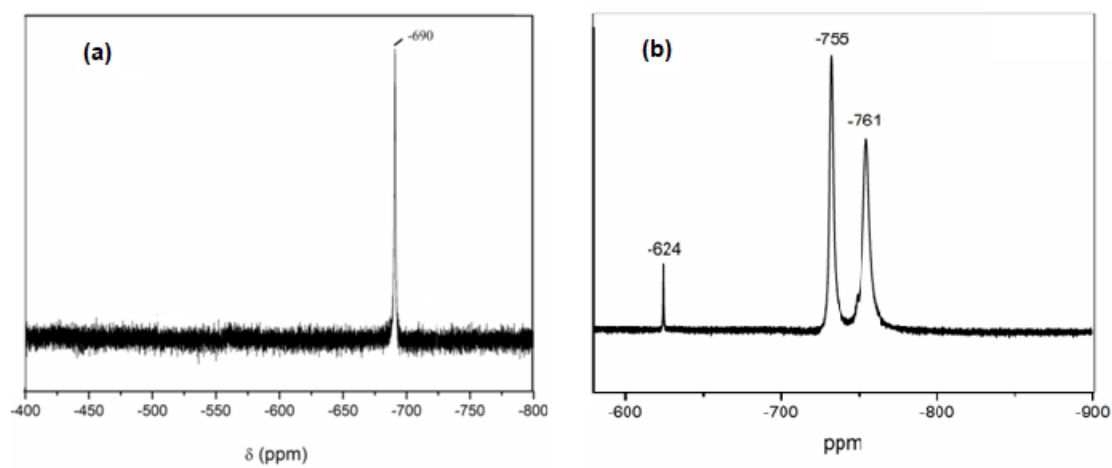


Fig. 19 ^{51}V NMR spectra of (a) ChpV and (b) PAmV in D_2O

Table 4 ^{13}C NMR spectral data for chitosan and chitosan anchored peroxidometal complex, **ChpV**

Compound	Chemical shift (ppm)				
	C-1	C-2	C-3–C-5	C-4	C-6
Chitosan	106.31	58.73	76.84	85.11	62.33
ChpV	100.51	57.78	76.84	85.81	62.74

Table 5 ^{13}C NMR chemical shifts for polymer anchored pV and pTa compounds- **PAmV**, **PATa** and **PSSTa**

Compound	Chemical shift (ppm)									
	Carboxylate carbon		CH	CH_2	Ring carbon					
	Free	Complexed			C1	C2	C3	C4	C5	C6
PAm	179.52		41.72	34.95						
PAmV	179.51	215.47	41.85	34.93						
PA	184.50		45.52	36.10						
PATa	184.91	215.54	45.90	36.11						
PSS	-	-	40.52	44.14	140.35	128.84	125.57	148.55	125.35	128.17
PSSTa	-	-	40.81	43.58	140.37	128.20	125.56	148.87	125.33	128.17

6.1.10 TG-DTG analysis

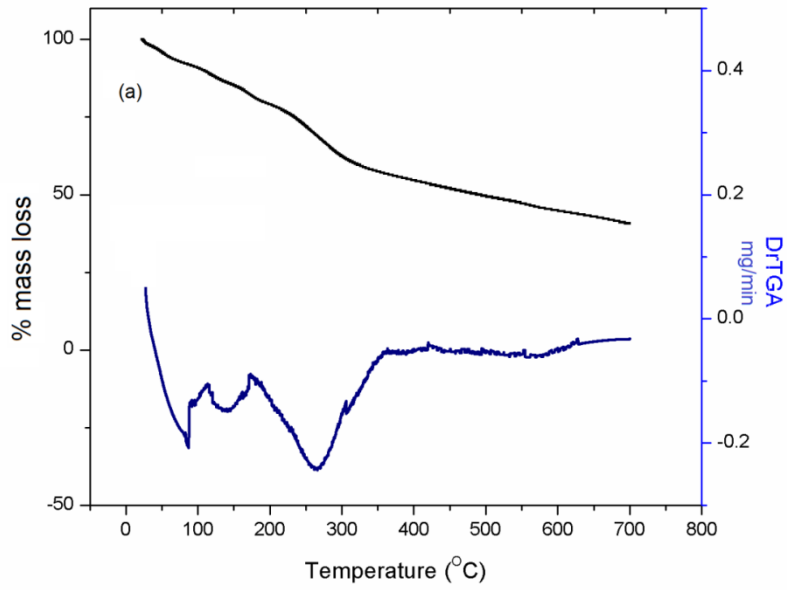


Fig. 20 TG-DTG plots of **ChpV**

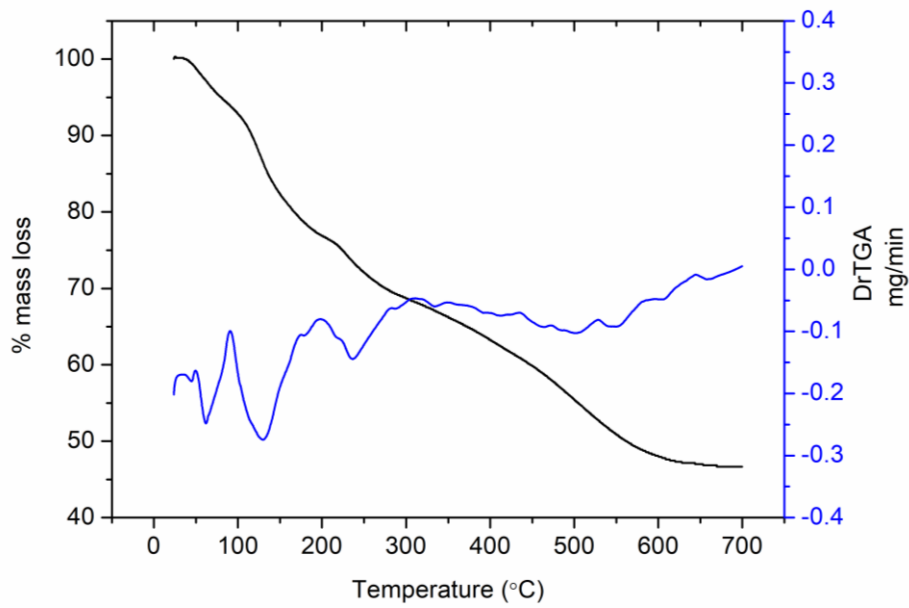


Fig. 21 TG-DTG plots of **PAmV**

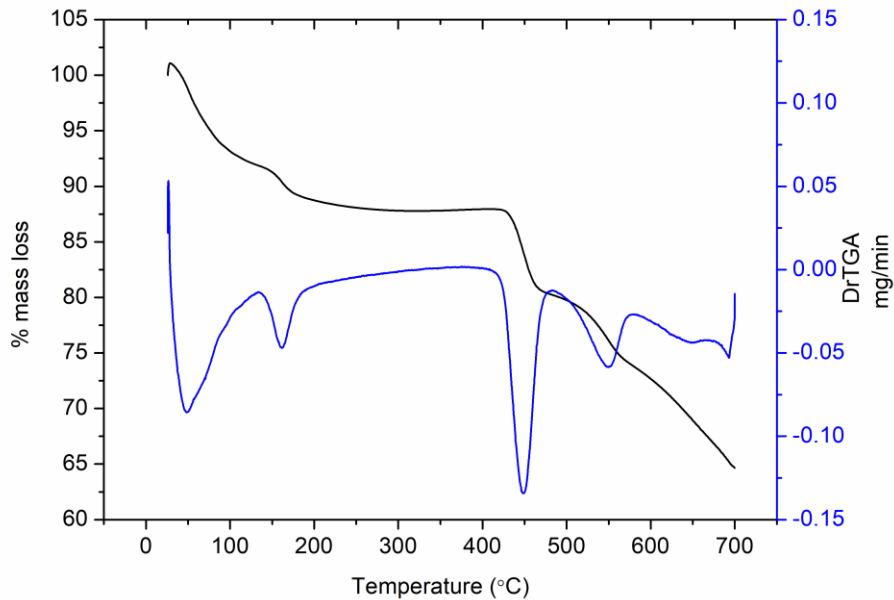


Fig. 21 TG-DTG plots of **PATa**

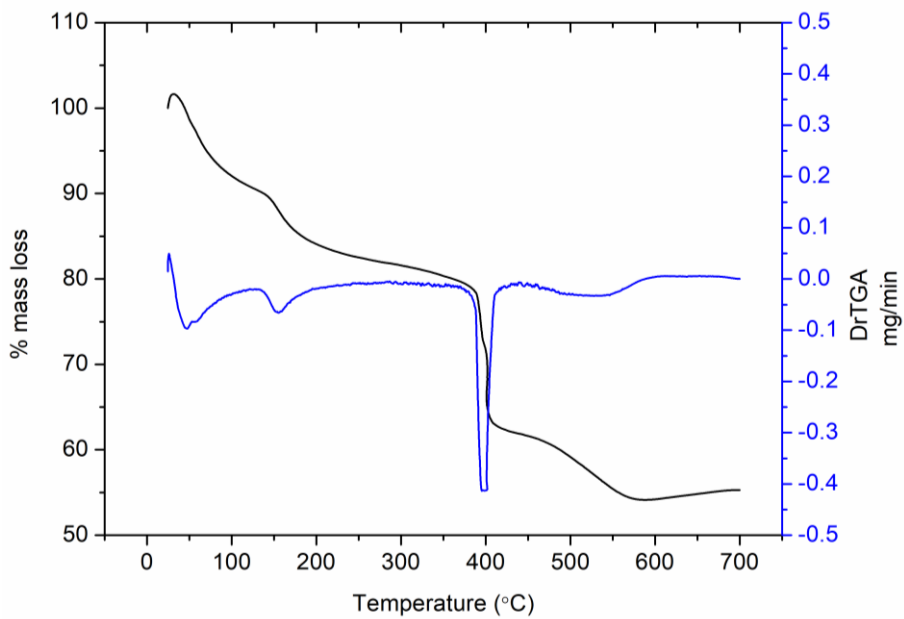


Fig. 22 TG-DTG plots of **PSSTa**

Table 6 TGA data for **ChpV**, **PAmV**, **PATa** and **PSSTa**

Compound	Temperature range (°C)	Observed weight loss (%)	Final residue(%)
ChpV	37-65	5.9	59.8
	139-182	12.7	
	226-310	21.6	
PAmV	35-92	6.3	46.2
	93-197	17.0	
	198-326	9.7	
	327-669	20.7	
PATa	40-90	8.0	54.7
	93-275	10.6	
	329-605	26.7	
PSSTa	41-110	7.4	65.4
	118-276	4.5	
	392-691	22.6	

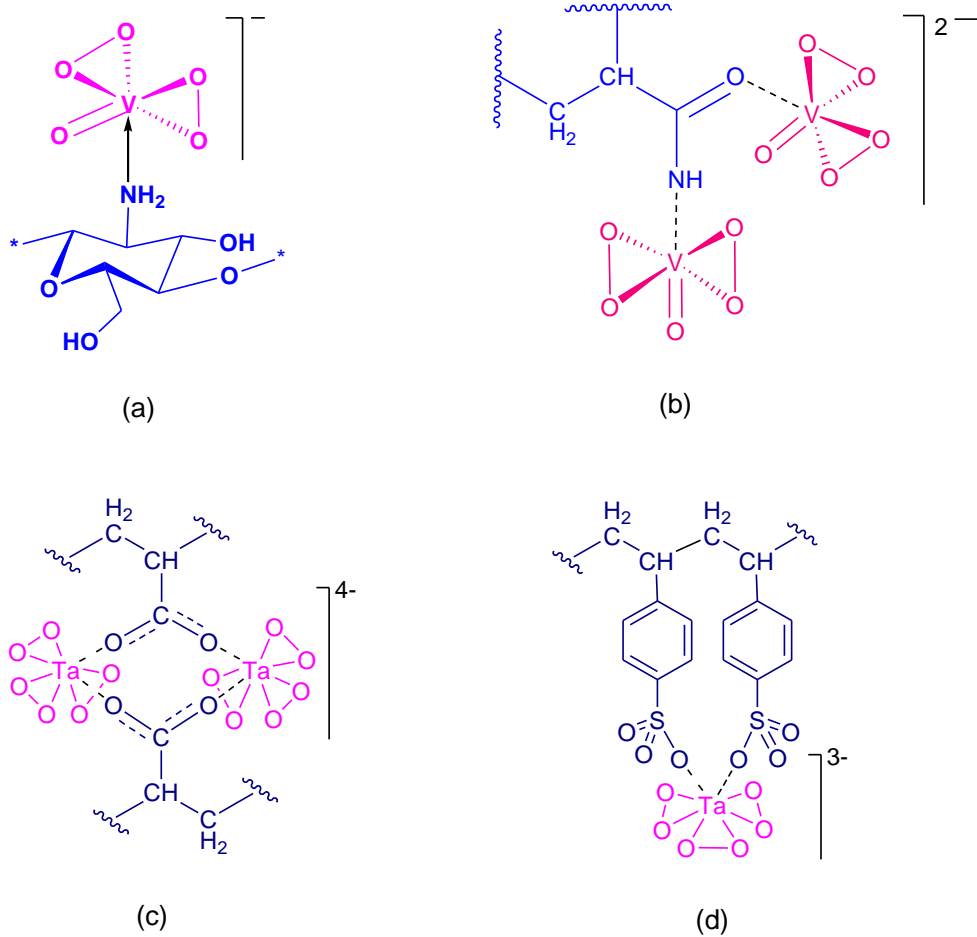


Fig. 23 Structures of (a) **ChpV**, (b) **PAmV**, (c) **PATa**, and (d) **PSSTa**

6.2 CATALYTIC ACTIVITY STUDY:

6.2.1 Catalytic activity of heterogeneous complex, ChpV

Table 7 Optimization of reaction conditions for selective oxidation of methyl phenyl sulfide (MPS) by 30% H₂O₂ catalyzed by **ChpV** complex^a

Reaction scheme: Cc1ccccc1S (1) $\xrightarrow[\text{Solvent, 30 \% H}_2\text{O}_2]{\text{ChpV}}$ Cc1ccccc1S(=O)C (1a) + Cc1ccccc1S(=O)(=O)C (1b)

Entry	Molar ratio (V:MPS)	H ₂ O ₂ (equiv.)	Solvent	Time (min)	Isolated yield (%)	1a: 1b	TON ^b	TOF ^c (h ⁻¹)
1	1:1000	2	H ₂ O	300	96	100:0	960	192
2	1:1000	3	H ₂ O	180	94	100:0	940	313
3	1:1000	4	H ₂ O	75	96	100:0	960	768
4	1:1000	5	H₂O	40	98	100:0	980	1462
5	1:1000	6	H ₂ O	25	98	76:24	760	1809
6	1:2000	5	H ₂ O	90	97	100:0	1940	1293
7	1:500	5	H ₂ O	30	95	82:18	410	820
8	1:1000	1	CH ₃ CN	120	94	100:0	940	470
9	1:1000	2	CH₃CN	30	95	100:0	950	1900
10	1:1000	3	CH ₃ CN	20	98	89:11	890	2696
11	1:500	2	CH ₃ CN	20	96	100:0	480	1454
12	1:1500	2	CH ₃ CN	70	97	100:0	1469	1259
13	1:2000	2	CH ₃ CN	130	95	100:0	1900	876
14	1:1000	2	MeOH	80	97	100:0	970	729
15	1:1000	2	EtOH	60	97	100:0	970	970
16 ^d	-	5	H ₂ O	40	11	78:22	-	-
17 ^d	-	2	CH ₃ CN	30	9	71:29	-	-
18 ^e	1:1000	5	H ₂ O	70	98	92:8	900	771
19 ^e	1:1000	2	CH ₃ CN	90	96	81:19	780	520

^aAll reactions were carried out with 5 mmol of substrate, 30% H₂O₂ in 5 mL of solvent. Catalyst (2.1 mg for 0.005 mmol of V). ^bTON (turnover number) = mmol of product per mmol of catalyst. ^cTOF (turnover frequency) = mmol of product per mmol of catalyst per hour. ^dBlank experiment without any catalyst. ^eUsing DPV as catalyst (0.8 mg, 0.005 mmol).

Table 8 Selective oxidation of sulfides to sulfoxides with 30% H₂O₂ catalyzed by **ChpV** in H₂O^a

Entry	Substrate	Time (min)	Isolated Yield (%)	TON ^b	TOF ^c (h ⁻¹)
1		40	98	980	1462
		40	96 ^d	960	1432
		40	97 ^e	970	1447
2		10	94	940	5628
3		30	95	950	1900
4		35	96	960	1646
5		50	97	970	1164
6		35	93	930	1595
7		75	94	940	752
8		150	96	960	384
9		360	39	390	65

^aAll reactions were carried out with 5 mmol substrate, 25mmol 30% H₂O₂ and catalyst (0.005 mmol of V) in 5 mL H₂O at RT. ^bTON (turnover number) = mmol of product per mmol of catalyst. ^cTOF (turnover frequency) = mmol of product per mmol of catalyst per hour. ^dYield of 3rd reaction cycle. ^eYield at scale-up reaction (7.5 g of MPS).

Table 9 Selective oxidation of sulfides to sulfoxides with 30% H₂O₂ catalyzed by **ChpV** in CH₃CN^a

Entry	Substrate	Time (min)	Isolated Yield (%)	TON ^b	TOF ^c (h ⁻¹)
1		30	97	970	1940
		30	96 ^d	960	1920
		30	93 ^e	930	1860
2		10	95	950	5688
3		20	94	940	2848
4		30	96	960	1920
5		70	97	970	829
6		25	94	940	2238
7		120	93	930	465
8		110	94	940	513
9		360	47	470	78

^aAll reactions were carried out with 5 mmol substrate, 10 mmol 30% H₂O₂ and catalyst (0.005 mmol of V) in 5 mL acetonitrile at RT. ^bTON (turnover number) = mmol of product per mmol of catalyst. ^cTOF (turnover frequency) = mmol of product per mmol of catalyst per hour. ^dYield of 5th reaction cycle. ^eYield of scale up reaction (7.5 g of MPS).

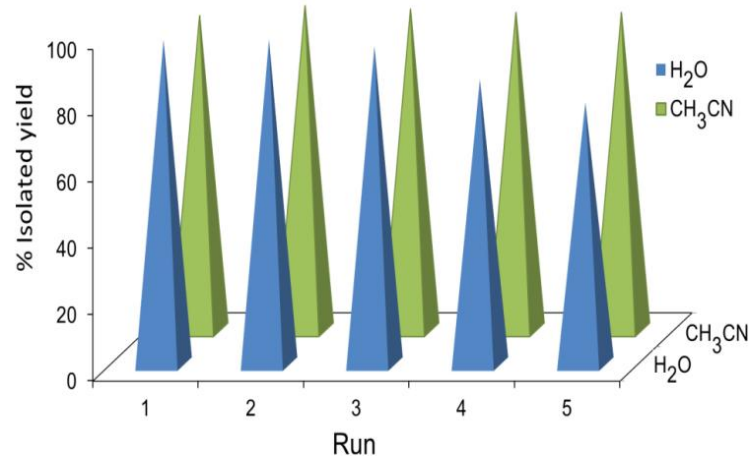


Fig. 24 Recyclability of **ChpV** for the selective oxidation of MPS to sulfoxide in H₂O and CH₃CN.

6.2.2 Catalytic activity of homogeneous complex, PAmV

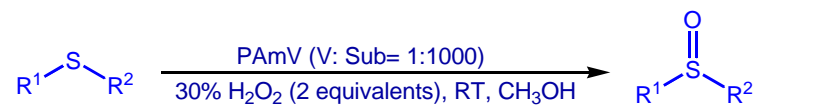
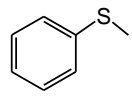
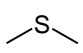
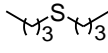
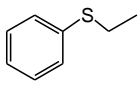
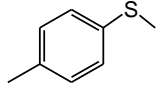
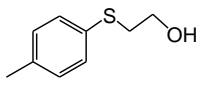
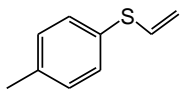
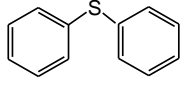
Table 10: Optimization of reaction conditions for selective oxidation of methyl phenyl sulfide (MPS) catalyzed by **PAmV** with 30% H₂O₂ as oxidant

The reaction scheme shows the oxidation of methyl phenyl sulfide (1) to methyl phenyl sulfoxide (1a) and methyl phenyl sulfone (1b). The reaction is catalyzed by PAmV in a solvent with 30% H₂O₂ as the oxidant.

Entry	Molar ratio (V:MPS)	H ₂ O ₂ (equiv.)	Solvent	Time (min)	Isolated yield(%)	1a:1b	TON	TOF (h ⁻¹)
1	1:1000	1	MeOH	90	96	100:0	960	640
2	1:1000	2	MeOH	15	97	100:0	972	3888
3	1:1000	2	EtOH	35	95	92:8	950	1638
4	1:1000	2	MeCN	25	96	100:0	960	2286
5	1:1000	2	H ₂ O	10	94	77:23	940	5628
6	1:1000	3	MeOH	10	97	81:19	970	5705
7	1:2000	2	MeOH	55	92	100:0	1840	2044
8	1:2500	2	MeOH	100	96	100:0	2415	1446
9 ^a	1:1000	2	MeOH	70	97	84:16	970	829
10 ^b	-	2	MeOH	15	6	88:12	-	-

^aUsing DPV as catalyst. ^bBlank experiment.

Table 11 Selective oxidation of sulfides to sulfoxides with 30% H₂O₂ catalyzed by PAmV^a

					
Entry	Substrates	Time (min)	Isolated yield(%)	TON ^b	TOF ^c (h ⁻¹)
1		15	97	972	3888
		15	97 ^d	970	3880
		15	95 ^e	950	3800
2		10	98	983	5782
3		15	97	970	3880
4		30	96	960	1920
5		15	97	970	3880
6		180	97	970	323
7		195	98	980	301
8		360	76	760	127

^aAll the reactions were performed with 5 mmol of substrate, 10 mmol of 30 % H₂O₂ in 5 mL of solvent at RT. Catalyst (1.6 mg, 0.005 mmol of V). ^bTON (turn over number)= mmol of product per mmol of catalyst. ^cTOF (turn over frequency)= mmol of product per mmol of catalyst per hour. ^d% Conversion for 3rd reaction cycle. ^eScale-up data. (7.5 g of MPS)

6.3 INVESTIGATION OF BIOCHEMICAL ACTIVITY OF THE COMPOUNDS

6.3.1 Stability of the compounds toward decomposition in solution with or without catalase

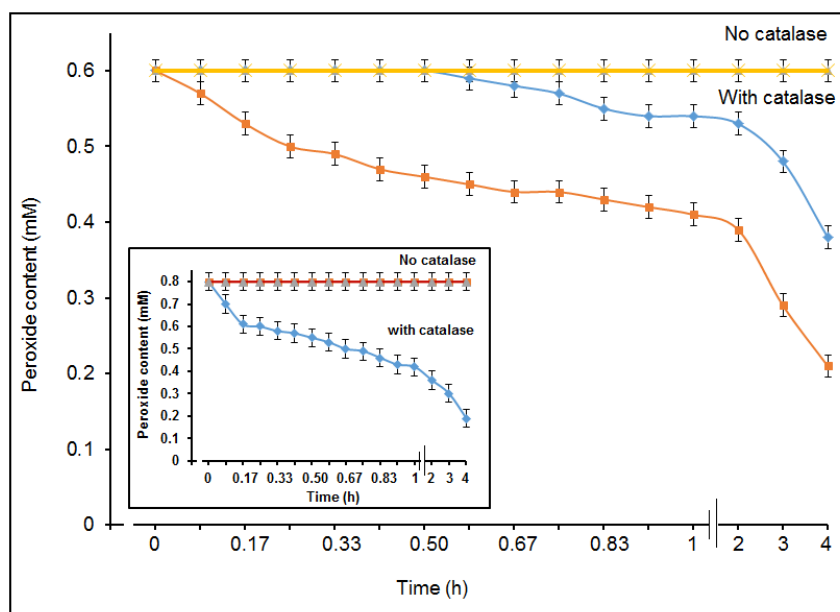


Fig. 25 Stability of compound **PATa** at different pH values: (\blacktriangle) compound solution in distilled water, pH of the solution = 9.0, (\times) solution of the complex in phosphate buffer (50 mM, pH 4.6). Stability of compound **TpTa** at different pH values: (\blacktriangle) compound solution in distilled water, pH of the solution = 10.0, (\blacksquare) solution of the complex in phosphate buffer (50 mM, pH 4.6) (inset). Effect of catalase on (\blacklozenge) **TpTa** (inset), (\blacklozenge) **PATa** and (\blacksquare) **PSSTa**. The reaction mixture contained phosphate buffer (50 mM, pH 7.0) and catalase enzyme (40 $\mu\text{g}/\text{mL}$) which was incubated at 30 $^{\circ}\text{C}$ for 5 min. The reaction was initiated after the addition of respective compounds, peroxide content of the aliquots drawn from the stock solution was determined at definite time intervals.

Table 12: Catalase dependant release of oxygen from pTa compounds

Entry	Compound	Concentration		Peroxide content (mM)	Loss of peroxide ($\mu\text{M}/\text{min}$)
		mg/mL	(mM)		
1	TpTa	0.792	0.2	0.8	2.54
2	PATa	0.123	0.2	0.6	0.92
3	PSSTa	0.235	0.2	0.6	1.63

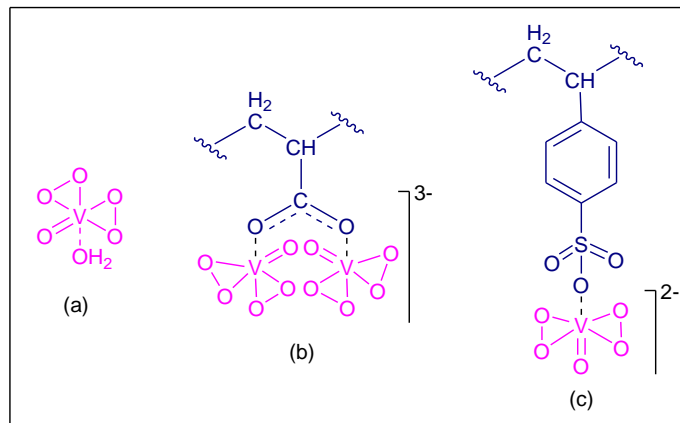


Fig. 26 Peroxido compounds of vanadium(V) under investigation for the present study: (a) **DPV**, (b) **PAV**, and (c) **PSSV**.

6.3.2 Effect of pV and pTa complexes on the activity of acid phosphatase

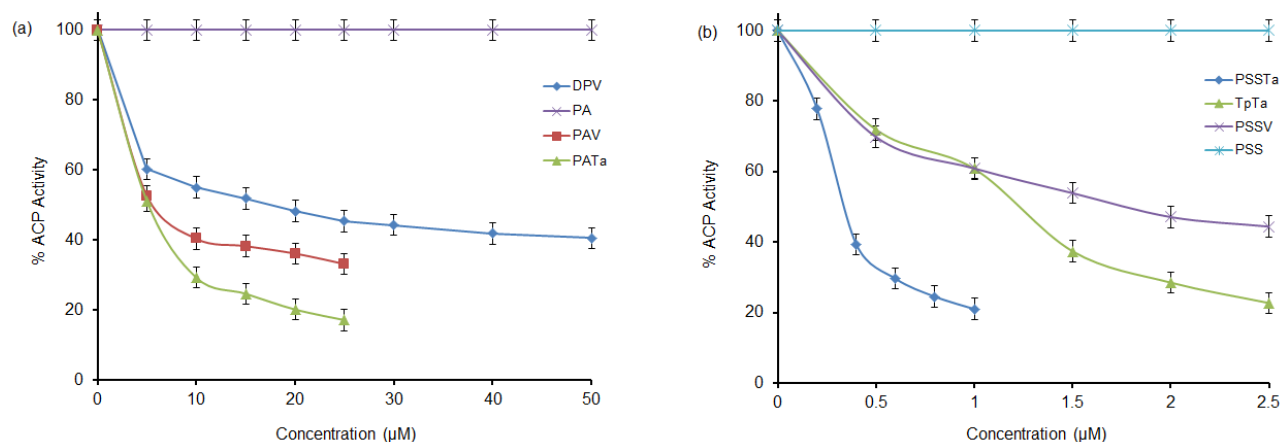


Fig. 27 The effect of neat homoleptic and polymer anchored peroxidometal compounds as well as free ligand on the activity of ACP. The ACP catalyzed rates of hydrolysis of *p*-NPP at pH 4.6 were determined at 30 °C by measuring A_{405} in a reaction mixture comprising of ACP ($18.38 \mu\text{g mL}^{-1}$) and *p*-NPP (2 mM) in acetate buffer (0.1 M, pH = 4.6) in absence or presence of stated concentrations of the inhibitors. (a) for **DPV** and the free ligand poly(sodium acrylate) (PA), concentrations are: 5, 10, 15, 20, 25, 30, 40 and 50 μM and for **PAV** and **PATa**, compound concentration: 5, 10, 15, 20 and 25 μM , (b) for **PSSV**, **TpTa** and free ligand poly(sodium 4-styrene sulfonate) (PSS), compound concentration: 0.5, 1, 1.5, 2.0 and 2.5 μM and for **PSSTa**, compound concentrations are: 0.2, 0.4, 0.6, 0.8 and 1.0 μM . The data are presented as the means \pm SE from three separate experiments. For polymeric compounds, the compound concentrations are on the basis of peroxidometal loading.

6.3.3 Kinetics of ACP inhibition by pV and pTa compounds

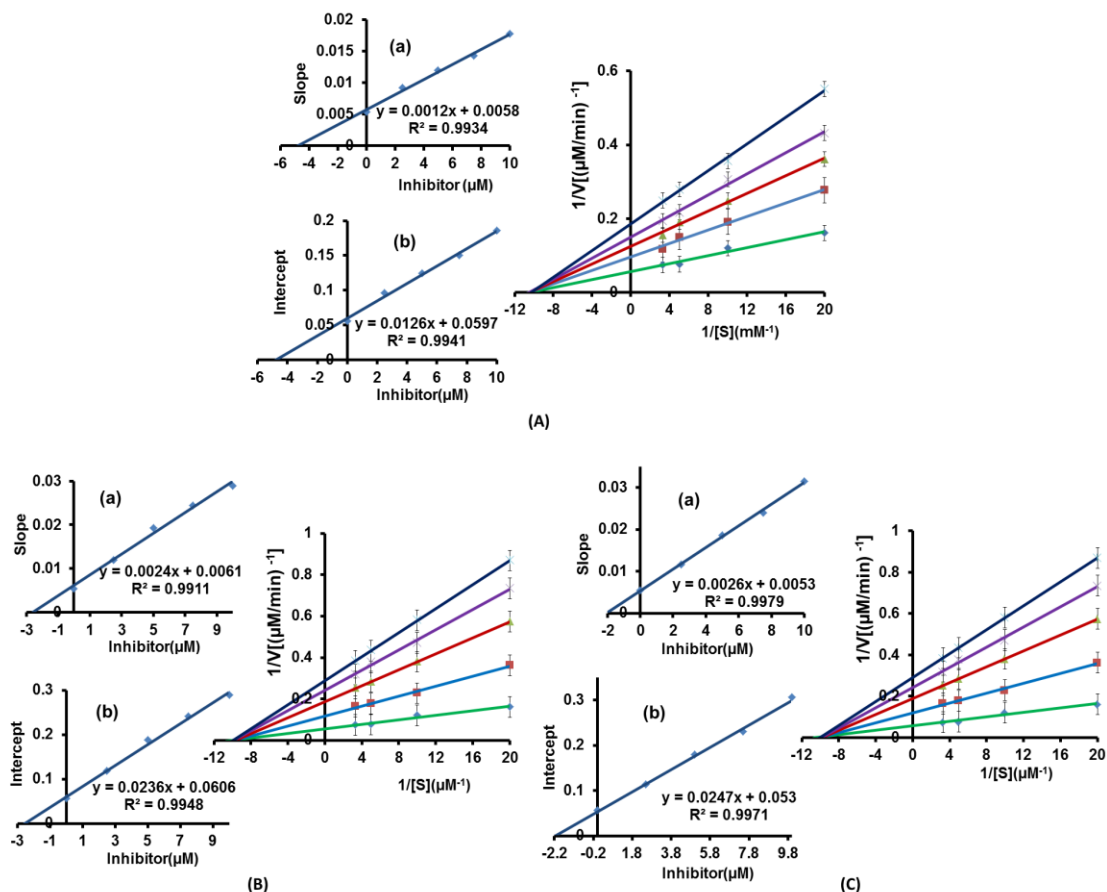


Fig. 28 Lineweaver-Burk plots for the inhibition of ACP activity in presence or absence of (A) **DPV**, (B) **PAV** and (C) **PATa**. The inset represents the secondary plot of the initial kinetic data of the Lineweaver-Burk plot. The reaction mixture contained acetate buffer (0.1 M, pH 4.6) and *p*-NPP (50-300 μM). The reaction was started by adding ACP (18.38 $\mu\text{g mL}^{-1}$) to the reaction solution, which was pre-incubated for 5 min and the rates of hydrolysis in the presence of \blacklozenge 0 μM , \blacksquare 2.5 μM , \blacktriangle 5 μM , \times 7.5 μM , \blacktimes 10 μM inhibitors were obtained. The values are expressed as the mean \pm SE from three separate experiments. Inset: (a) the slopes were plotted against inhibitor concentrations and K_i values were obtained from the x-intercepts of these re-plots. (b) The vertical intercepts were plotted against the inhibitor concentration and K_{ii} values were obtained from the x-intercepts of these re-plots.

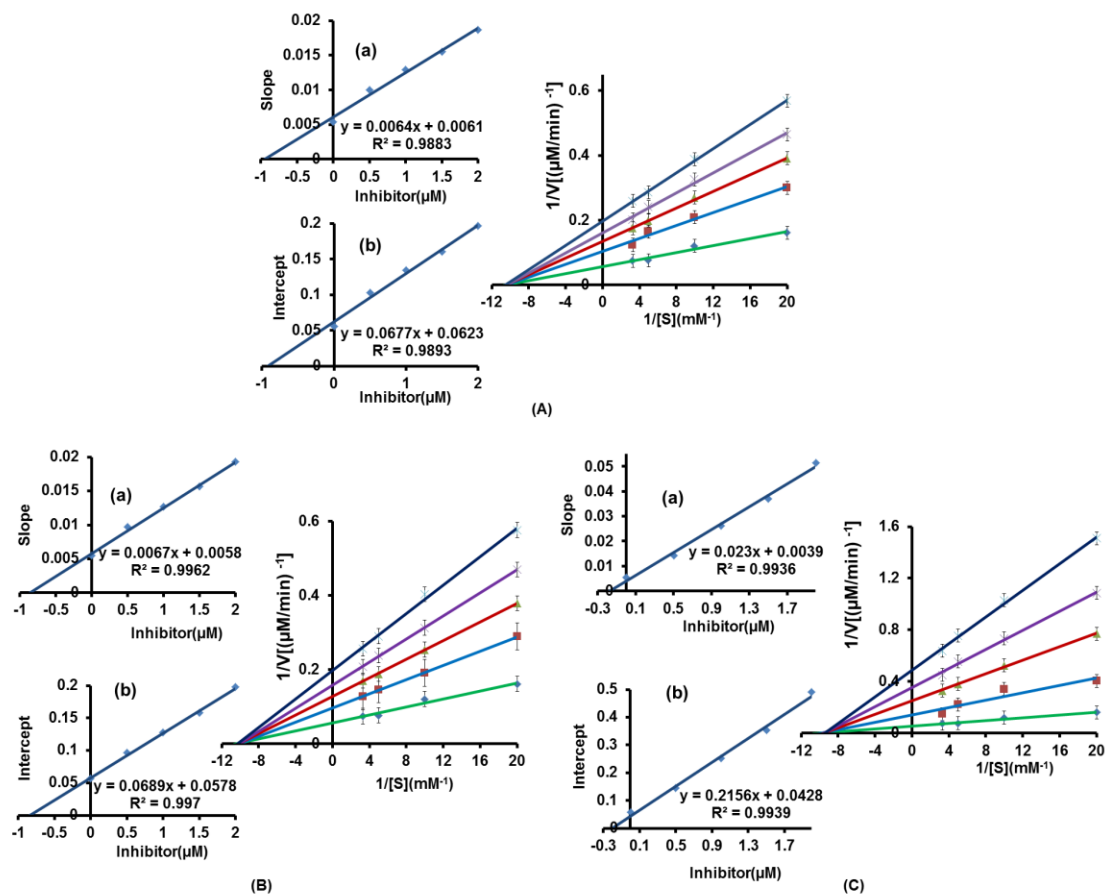


Fig. 29 Lineweaver-Burk plots for the inhibition of ACP activity in presence or absence of (A) **TpTa**, (B) **PSSV** and (C) **PSSTa**. The inset represents the secondary plot of the initial kinetic data of the Lineweaver-Burk plot. The reaction mixture contained acetate buffer (0.1 M, pH 4.6) and *p*-NPP (50-300 μM). The reaction was started by adding ACP (18.38 μg mL⁻¹) to the reaction solution, which was pre-incubated for 5 min and the rates of hydrolysis in the presence of ♦ 0 μM, ■ 0.5 μM, ▲ 1.5 μM, X 2 μM, ✕ 2.5 μM inhibitors were obtained. The values are expressed as the mean ± SE from three separate experiments. Inset: (a) the slopes were plotted against inhibitor concentrations and K_i values were obtained from the x-intercepts of these re-plots. (b) The vertical intercepts were plotted against the inhibitor concentration and K_{ii} values were obtained from the x-intercepts of these re-plots.

Table 13: Half-maximal inhibitory concentration (IC_{50}) and inhibitor constants (K_i and K_{ii}) values for pV and pTa compounds

Compound	IC_{50} (μM)	K_i (μM)	K_{ii} (μM)	K_{ii}/K_i	Types of inhibition
DPV	16.79	4.71	4.70	0.99	Non-competitive inhibition
TpTa	1.77	0.94	0.91	0.97	Non-competitive inhibition
PAV	5.64	2.5	2.5	1.00	Non-competitive inhibition
PATa	5.06	2.0	2.2	1.10	Non-competitive inhibition
PSSV	1.22	0.82	0.82	1.00	Non-competitive inhibition
PSSTa	0.34	0.16	0.17	1.06	Non-competitive inhibition

Note: ACP catalyzed rates of hydrolysis of *p*-NPP at pH 4.6 were determined at 30 °C by measuring A_{405} in a reaction mixture containing ACP ($18.38 \mu\text{g mL}^{-1}$) and *p*-NPP (50-300 μM) in acetate buffer (0.1 M, pH = 4.6) in the presence of stated concentrations of the inhibitors.

ANNEXURE II

1. Characterization of the newly synthesized macrocomplexes

1.1 Elemental Analysis

The elemental analysis data complemented by inductively coupled plasma-optical emission spectrophotometric (ICP-OES) analysis and EDX spectral analysis results showed the metal and peroxide ratio as well as respective metal loading on polymer support. The metal: peroxide ratio was found to be 1:2 for peroxidovanadium (pV) complexes (**ChpV** and **PAmV**) and 1:3 for peroxidotantalum (pTa) complexes (**PATa** and **PSSTa**). The metal loading (V or Ta) on the polymeric support was found to be 2.34, 3.06, 1.62 and 0.85 mmol^g⁻¹ for **ChpV**, **PAmV**, **PATa**, and **PSSTa** complexes, respectively.

1.2 SEM and Energy Dispersive X-ray Analysis

The scanning electron micrographs of the compounds showed considerable roughening of the surface compared to the free polymers as seen in **Fig. 1**. This morphological change of the surface of the compounds is due to the adsorption or dispersion of the peroxidometallates on the pristine polymer surface.

The presence of K and V along with C, O and N in the supported pV catalyst, **ChpV** has been confirmed from the energy dispersive X-ray analysis results. The energy dispersive X-ray analysis data clearly revealed the presence of V in **PAmV** in addition to C, O, N, Na [**Fig. 2(b)**]. The spectra [**Fig. 2(c),(d)**] also showed C, O, Na, Ta as constituents of the compounds **PATa** and **PSSTa**. The existence of S in the compound **PSSTa** was also confirmed from its EDX spectrum [**Fig. 2(d)**]. The composition of the compounds derived from EDX analysis data presented in **Table 1**, agreed well with the results obtained from elemental analysis.

1.3 X-ray diffraction studies

The X-ray diffraction patterns of chitosan and metal incorporated polymer immobilized complex, **ChpV** are presented in **Fig. 3**. The X-ray diffractogram of chitosan displayed three main diffraction peaks at 2 Θ values of *ca.* 12.7, 19.97 and 26.7° respectively, which correspond to the semi-crystalline nature of the polymer [6]. In the diffractogram of the complex, intensities of the characteristic peaks of chitosan were observed to weaken with concomitant appearance of many new diffraction peaks, indicative of the formation of a new crystalline phase [7]. The decrease in intensity of the peaks corresponding to chitosan is likely to be due to the disruption of hydrogen bonds within chitosan owing to incorporation of metal complex [7b, 8]. This may be a plausible factor responsible for relatively lower thermal stability of the complex as has been demonstrated by TGA results. The additional sharp diffraction peaks in the diffractogram of **ChpV** complex, were located at 2 Θ values of 14.4, 15.3, 17.7, 25.2 and 28.6°. These values are close to the ones observed for peroxidovanadium species (PDF 81-2392) and may be ascribed to

the (001), (200), (201), (110) and (202) planes, respectively. These findings confirmed the anchoring of peroxidometal moieties to the polymer matrix.

1.4 X-ray photoelectron spectroscopy

The XPS spectrum of **ChpV** is presented in **Fig. 4**. This technique is important for analyzing the electronic properties of the species on the surface. The complex **ChpV** displayed characteristic peaks of vanadium ($2p_{3/2}$ and $2p_{1/2}$) at 517.5 and 525.0 eV, respectively with a difference of splitting of *ca.* 7.5 eV which is close to the value reported for V_2O_5 [9]. The binding energy values suggest the presence of vanadium at + 5 oxidation state in the complex on the basis of available literature [9-10]. Thus, XPS study confirmed the immobilization of peroxidometallate complex on chitosan.

1.5 BET Analysis

The surface area of the polymer, chitosan and metal incorporated complex, **ChpV** were measured by using BET analysis with nitrogen adsorption method and pore volume was determined by BJH model [11]. The N_2 adsorption/desorption isotherm of the compound showed typical type II adsorption (**Fig. 5**) of an IUPAC standard on particles which have macropores or nonpores showing poor adsorption [12]. The average specific surface area of the supported metal complex was found to be $43.6 \text{ m}^2/\text{g}$ which is considerably greater than that of the pristine polymer ($3.0 \text{ m}^2/\text{g}$) (**Table 2**). Thus it is evident that complexation of chitosan with the metal, vanadium resulted in affirmative changes in surface morphology of the polymer. The value of the constant C in the BET equation was in the range (2-200) which is characteristic of a multilayer adsorption (type II isotherm) [13].

1.6 IR and Raman spectral studies

The IR and Raman spectra of the complexes are presented in **Fig. 6-13**. Characteristic differences were observed in the spectral pattern of the metal incorporated polymer complexes compared to the pure polymer, indicated successful anchoring of the peroxidometallate species on the polymer matrix.

As seen in **Fig. 6**, the IR spectrum of initial free chitosan exhibited typical peaks located approximately at 3434 (O-H stretch and N-H stretch), 2921 ($-\text{CH}_3$ stretch), 2876 ($-\text{CH}_2$ stretch), 1592 (N-H bending) and 1154 (bridge O stretch) [8a,14], 1646 cm^{-1} (C–O stretching along with N–H deformation mode, amide I) [7b,15]. The metal incorporated compound, **ChpV** did not show any distinct shift in the position of amide I band of the complex compared to the untreated polymer indicating that the amide group is not involved in co-ordination with the metal. The possibility of co-ordination through N atom of the amide group is also not likely as such co-ordination causes a considerable decrease in the carbonyl stretching frequency which is not the case for the complex [16]. The peak at 3434 cm^{-1} corresponding to the stretching vibration of $-\text{NH}_2$ and $-\text{OH}$ group showed a considerable shift to the lower frequency suggesting that either $-\text{NH}_2$ or $-\text{OH}$ group takes part in complexation [7a,7c,8a,14,17]. However, the peak attributed to the bending vibration of the $-\text{OH}$ group at 1421 cm^{-1} and the band assigned to primary and

secondary –OH group at 1038 and 1089 cm^{-1} , respectively remained unaltered in the spectrum of **ChpV** complex, negating the possibility of –OH group taking part in chelation [7c,14,17-18]. The –NH bending vibration of the free amine group in chitosan is shifted to the lower wavenumber in **ChpV**. Thus, it was observed that both stretching and bending vibration of –NH₂ group shifted to the lower value in the complex, because co-ordination of the chitosan through nitrogen centre with metal ion would possibly reduce the electron density of the amino group [7a-c,8a,15a,17]. This confirmed the co-ordination of vanadium (V) with chitosan through –NH₂ group. The characteristic bands of chitosan, β -(1–4) glycoside bridge bands (at around 1,154 and 894 cm^{-1}) were also seen in the FT-IR spectra of the complex, indicating that the metal complex successfully anchored to chitosan without altering the main backbone of chitosan [7b,8b,15c,19].

The IR spectrum of the pure polymer, poly(acrylamide) displayed typical vibrations at 3399, 3197 (–NH stretching), 1664 (–C=O stretching, amide I), 1615 (–NH₂ bending, amide II) and 1452 cm^{-1} (C–N stretching)[20]. After metal incorporation, the absorption band assigned to –C=O stretching (amide I) shifted to lower value indicating involvement of carbonyl group in metal co-ordination [21]. The disappearance of the band assigned to –NH₂ bending vibration (amide II) in the spectrum of the complex, **PAmV** suggested a possibility of simultaneous co-ordination of N-atom of amide to vanadium centre [22]. There have been reports showing occurrence of simultaneous co-ordination of two donor sites of acrylamide where the ligand acts as a bridge between the two bonded metal atoms [23]. The –NH₂ stretching vibration could not be assigned with certainty in the metal complex due to the overlapping with the intense band at around 3400 cm^{-1} for the presence of water molecules in the complex.

Apart from the typical polymer absorptions, in case of both pV complexes, additional bands of the metal-peroxido specie were seen in the vicinity of 860, 600 and 530 cm^{-1} assigned to the $\nu(\text{O-O})$, $\nu_{\text{as}}(\text{V-O}_2)$ and $\nu_{\text{s}}(\text{V-O}_2)$ modes, respectively, whereas the terminally bonded V=O group was observed near 930 cm^{-1} (**Fig. 6** and **7**) [21a,24]. In the Raman spectra, the bands attributable to $\nu(\text{O-O})$, $\nu_{\text{as}}(\text{V-O}_2)$, $\nu_{\text{s}}(\text{V-O}_2)$ and $\nu(\text{V=O})$ were seen at around 890, 625, 530 and 960 cm^{-1} for both the complexes, respectively (**Fig. 10** and **11**).

For peroxidotantalum complexes, three absorptions corresponding to $\nu(\text{O-O})$ vibration were observed in the 800-840 cm^{-1} region depicting the presence of three peroxido groups per metal centre in case of both **PATa** and **PSSTa** (**Fig. 8** and **9**) [25]. In addition to this, $\nu_{\text{as}}(\text{Ta-O}_2)$ and $\nu_{\text{s}}(\text{Ta-O}_2)$ absorptions were detected in 500-600 cm^{-1} range (**Fig. 8** and **9**) [25]. The Raman spectra of the complexes complimented the IR results by displaying bands for $\nu(\text{O-O})$, $\nu_{\text{as}}(\text{Ta-O}_2)$ and $\nu_{\text{s}}(\text{Ta-O}_2)$ in the respective region shown in **Table 3**.

The available literature pertaining to metal-carboxylate co-ordination shows that $\Delta\nu = \nu_{\text{as}}(\text{COO})-\nu_{\text{s}}(\text{COO})$ relationship has been derived as an important criterion to determine the mode of carboxylate binding to a metal centre [21a,26]. The IR spectrum of the complex **PATa** displayed typical bands for $\nu_{\text{as}}(\text{COO})$ and $\nu_{\text{s}}(\text{COO})$ modes at 1574 cm^{-1} and 1409 cm^{-1} respectively as shown in **Fig. 5.5(b)**, while that of free PA were observed at 1565 cm^{-1} and 1409 cm^{-1} . The $\Delta\nu$ (165 cm^{-1}) value obtained from the spectrum of **PATa** is close to that observed for

free PA ($\Delta\nu = 157 \text{ cm}^{-1}$), which suggests bridging bidentate mode of co-ordination of the carboxylate group [21a,26-27]. An additional IR band observed in the region of 1713 cm^{-1} indicated the existence of free carboxylic acid group in the complex [21a].

The IR spectrum of the pure polymer, PSS has shown bands at 1197 and 1039 cm^{-1} representing ν_{as} and $\nu_{\text{s}}(\text{S-O})$ stretching modes of the pendant sulfonate group [21a,28]. After complexation, in addition to the symmetric stretching band at 1038 cm^{-1} , a distinct splitting pattern was observed at 1218 and 1183 cm^{-1} in the spectrum of **PSSTa** (**Fig. 9**) which may be attributed to the complexed sulfonate group [21a]. The appearance of the vibration at 1218 cm^{-1} in the complex denoted the existence of free sulfonate group [21a]. The characteristic absorptions of the phenyl group and CH_2 bending were exhibited at 1639 and 1496 cm^{-1} respectively.

1.7 Electronic spectral studies

The diffuse reflectance UV-visible spectrum of the compound **ChpV** showed two bands at around 350 and 245 nm (**Fig. 14a**). The band appearing at $350\text{-}380 \text{ nm}$ is assigned to peroxido to metal transition (LMCT) which is characteristic of peroxidometal species of vanadium(V) and tantalum(V) as well [24a,29]. The band at 245 nm is assigned to the typical $\text{n}\rightarrow\pi^*$ and $\pi\rightarrow\pi^*$ transitions of chitosan support [8a,17b,30].

The UV-Vis spectra of water soluble polymer supported pV and pTa complexes were recorded in aqueous solution. The spectrum of **PAmV** displayed a weak intensity band at around 320 nm which is typical of peroxido to metal (LMCT) transition of diperoxidovanadate species (**Fig. 14b**) [24a,29,31]. In case of polymer bound pTa complexes [**Fig. 14c,d**], the broad band observed in the $220\text{-}300 \text{ nm}$ region has been ascribed to tantalum-peroxido species ($\text{Ta}(\eta^2\text{-O}_2)$) on the basis of available literature reports [32].

1.8 ^{13}C NMR studies

The ^{13}C NMR spectrum of the compound, **ChpV** along with the spectrum of free chitosan recorded in the solid state is presented in **Fig. 15**. The corresponding resonances are listed in **Table 4** for comparison. The assignments are on the basis of available literature data [33]. However, exact resonance position may vary slightly according to the NMR technique used (solid or liquid state analysis). The ^{13}C NMR spectrum of chitosan displays characteristic resonances at 58.73 , 62.33 , 85.11 and 106.31 ppm attributable to C-2, C-6, C-4, and C-1 carbon atoms, respectively. The resonance centred at 76 ppm probably originates due to a combination of C-3 and C-5 signals as has been reported [33e]. As the chitosan used was highly deacetylated, no observable peaks at around 174 and 24 ppm characteristic of carbon atoms of -C=O and -CH_3 groups were found in the spectrum, as anticipated [33b,c]. The ^{13}C NMR spectra of the supported metal complexes showed distinct shift of the resonance positions of the carbon atoms of chitosan along with the broadening of the signals in comparison to the original chitosan spectrum indicating change in environment of C atoms after metal anchoring [33c,d]. The comparison of NMR spectra before and after loading of pV moiety showed considerable changes

in the spectrum of the compound (as seen in **Table 4**), although the overall spectral pattern of **ChpV** resembled closely the spectrum of free chitosan by exhibiting major peaks at 57.78, 62.74, 85.81 and 100.51 ppm due to C-2, C-6, C-4, and C-1 carbon atoms. The intensity of the signal corresponding to C-2 atom attached to the $-\text{NH}_2$ group was shifted by nearly 1 ppm and appeared as a weaker intensity shoulder along with the peak at 62.74 ppm in the spectrum of the compound which suggested the vanadium anchoring through $-\text{NH}_2$ group. Moreover, the considerable shifting of C-1 signal in the spectra of the complex indicated that amino and hydroxyl groups are not the only sites which were affected by the interaction with the metals. It is significant to note that no new resonance was seen in the spectrum at around 175 ppm, attributable to $-\text{COOH}$ group. Thus from the NMR analysis it has been confirmed that although the chitosan structure undergoes modification owing to anchoring of the peroxidometal species, however the main backbone structure of chitosan did not change during complexation with V(V) [34].

^{13}C NMR spectral analysis plays a decisive role in determining the mode of co-ordination of the macromolecular ligands to the metal centres. The ^{13}C NMR data of the polymer bound metal complexes as well as that of the pure polymers are presented in **Table 5**. The spectrum of the free poly(acrylamide) displayed expected resonances of the chain carbon atoms at 34 and 41 ppm along with resonance due to amide carbon atom at 179 ppm (**Fig. 16a**) [21a,35]. After metal incorporation, a new signal appeared at 215 ppm in addition to the peak at 179 ppm which was ascribed to the complexed amide group. The significant downfield shift of $\Delta\delta$ ($\delta_{\text{complex}} - \delta_{\text{free carboxylate}}$) \approx 36 ppm confirmed the metal co-ordination through the amide carbon [21a,36].

The spectrum of pure poly(sodium acrylate) showed, apart from the signals due to the $-\text{CH}_2$ and $-\text{CH}$ groups of the polymer chain, peaks due to C atom of carboxylate groups centred at 184 and 183 ppm (**Fig. 17a**) [21a,37]. Two closely spaced peaks observed in this region are likely to be due to the presence of carboxylate as well as $-\text{COOH}$ groups of the polymer in solution. The spectrum of the polymeric complex, **PATa** displayed an additional peak at 215 ppm attributable to the complexed carboxylate group [21a,38]. The downfield shift of $\Delta\delta$ ($\delta_{\text{complex}} - \delta_{\text{free carboxylate}}$) \approx 31 ppm of the compound was observed which is in accord with the previously obtained values for other polyacrylate incorporated peroxidometal compounds bonded in a bidentate fashion [21a,38]. This suggested the successful anchoring of the monomeric metal complexes on the poly(sodium acrylate) through the pendant carboxylate group.

The ^{13}C NMR spectral pattern of **PSSTa** complex shown in **Fig. 18**, remained practically unchanged after complexation *vis-a-vis* the virgin polymer spectrum. Since the Ta(V) centres are linked to the polymer through the pendant sulfonate groups which are well separated from the chain and ring carbon atoms of the polymer matrix, the above observation is not unexpected.

1.9 ⁵¹V NMR study

Further information regarding the co-ordination environment of the compounds **ChpV** and **PAmV** was derived from the ⁵¹V NMR spectral analysis. The spectrum of the compound, **ChpV** shown in **Fig. 19a**, displayed a resonance at – 690 ppm which is in the region typical of a diperoxidovanadate species. The peak has been assigned on the basis of available literature [21a,29,39].

The ⁵¹V spectrum of the compound, **PAmV** displayed major peaks at δ -761 and -755 ppm which is in the range observed for diperoxidovanadium complex in different ligand environment [21a,40]. Thus, the appearance of two major peaks in close proximity suggested the complexation of V through two binding sites of acrylamide. ⁵¹V NMR study thus provided further evidence in support of occurrence of vanadium in the compound bonded *via* both the binding sites of acrylamide *viz.*, -C=O and -NH₂ groups, as has been indicated by its IR spectral analysis. A relatively weaker intensity peak was also observed at -624 ppm which indicated the presence of traces of monoperoxidovanadate, probably resulting from the elimination of a peroxido group from the diperoxidovanadium moiety.

1.10 TG-DTG analysis

The TG-DTG plots along with the thermogravimetric analysis data of the polymer bound compounds are presented in **Fig. 20-23** and **Table 6**, respectively. The compounds underwent multistage degradation upon heating up to 700 °C. It is noteworthy that the immobilized pV and pTa complexes did not explode on heating. The first stage of degradation due to the release of water of crystallization occurs between room temperature and *ca.* 110 °C for the complexes. This was followed by the decomposition of peroxido groups in the subsequent step. Complete loss of peroxido groups from the compounds was confirmed from the absence of peroxido band in the IR spectra of the degraded product isolated at this stage.

In case of **ChpV**, apart from the initial water loss stage below 100 °C, chitosan exhibited single stage decomposition in the range of 270-315 °C with mass loss of 33.1% due to the degradation of the polymer including deacetylation. The polymer undergoes further degradation up to 700 °C. In majority of reports, it has been observed that complexation of chitosan with metal usually lowers the thermal stability of the polymer [7b,d,8b,c,17a,42]. In case of the chitosan anchored pV compound after the loss of peroxido groups, the compound undergo further degradation in the range of 203-581°C due to the cleavage of glycosodic linkage in the chitosan backbone [7b,8c]. Thus the step corresponding to degradation of the chitosan support occurs at a lower temperature in the compound, compared to free chitosan, indicating relatively lower thermal stability of the metal anchored chitosan complex, in agreement with the previous findings [7b,d,8b,c,17a,42]. The black residue remaining after complete degradation of the complex, **ChpV** was found to be 59.8%. FTIR spectrum of the residue displayed the typical $\nu(\text{M}=\text{O})$ bands of oxidovanadium species. The chitosan bands of the original compound nearly disappeared in the spectrum of the residue, which is in accord with previous report showing that the characteristic bands of chitosan disappear in the char residue obtained after thermal

degradation of chitosan on heating up to a temperature of 600 °C [43]. Thus it has been confirmed that the residue from the chitosan immobilized peroxidometallate complexes consisted of metal oxide along with the char residue of the polymer.

The compound, **PAmV** showed two stages of degradation after the loss of peroxido group. The first stage of degradation was seen in 198-326 °C range due to the release of water, ammonia and a small amount of carbon dioxide from the amide group while keeping the polymer chain intact [21a,44]. The breakdown of main polymer matrix occurred in the subsequent decomposition step in the range 327-669 °C. The residual mass of 46.2% retained after degradation up to 700 °C suggested reduced rates of degradation in comparison to the pure polymer [44,45] which is in accordance with the literature findings on TGA analysis of metal polyacrylamide complexes [46]. IR spectral analysis of the residue indicated the presence of oxido species of vanadium along with conjugated C=C bonds in the polymer chain as well as some residual nitrile functions [44].

On heating of the complex **PATa** after the initial loss of peroxido groups, leads to its further decomposition in the temperature range of 329-605 °C which may be attributed to the decarboxylation and breakage of the polymer chain [21a]. The TG-DTG profile of **PATa** agreed well with the previously reported thermogravimetric analysis of other polyacrylate anchored peroxidometal compounds [3c,21a,24a,38a]. The residue after complete degradation of **PATa** was found to be 54.7 %. FT-IR spectral analysis of the residual mass was carried out which showed bands at 867 cm⁻¹ and 611 cm⁻¹ suggesting the existence of tantalum oxido group in the residual moiety [47]. Along with that, an additional band at 1443 cm⁻¹ was observed which may be ascribed to sodium carbonate species present in the residue along with oxidotantalate [11]. It has been reported earlier that thermal decomposition of sodium acrylate produce sodium carbonate in addition to CO₂ and CO as final decomposition product [48].

In case of **PSSTa**, two stages of degradation was observed in the temperature range of 400-697 °C after the initial dehydration step and the complete loss of peroxido group. This may be ascribed to the loss of sulfonate group as well as the rupture of polymer chain with the release of ethylene, water, SO₂ and CS₂ along with other products as mentioned in literature [49]. The thermal degradation of sodium poly(styrene 4-sulfonate) in the temperature range of 450-550 °C was observed due to polystyrene as well as -SO₃Na group decomposition, while in the temperature range of 550-580 °C, CO evolves along with an alcohol [49]. The total weight loss of the compound **PSSTa** after complete degradation up to 700°C was found to be 34.5 %. The IR spectral analysis of the residual mass suggests the existence of oxidotantalate group. The appearance of the band at 1642 and 1124 cm⁻¹ is indicative of sodium sulphate group present in the residue [49,50]. Thus, TG-DTG analysis provides additional evidences in support of the composition and formula proposed for the newly synthesized compounds.

The above information is consistent with proposed structures of the type schematically illustrated in the below figure for the newly synthesized compounds **ChpV**, **PAmV**, **PATa** and **PSSTa**.

Based on these data, proposed structures applicable to the complexes **ChpV**, **PAmV**, **PATa** and **PSSTa** are shown schematically in **Fig. 23**. Different models have been proposed previously [7a,17a] to describe the mode of metal ion-chitosan co-ordination such as ‘bridge model’ and ‘pendant model’. In the bridge model, the metal ion is usually bound with four nitrogen atoms from the same chain or from different chains; whereas, in the pendant model the metallic ion is linked to the amino group as pendant. Thus the proposed structure for **ChpV** show co-ordination of the V(V) to the amino group of chitosan polymer to form a ‘pendant’ complexes. The peroxidovanadium complex, **PAmV** is proposed as a six co-ordinated compound with each metal centre containing one oxido and two peroxido groups, where the polymeric ligand is co-ordinated through either $-NH_2$ or $-C=O$ group. Such type of bonding is not unprecedented as there are available reports on metal complexation through the multiple donor sites of acrylamide [23]. For **PATa** complex, carboxylate group of poly(acrylate) chain binds to the metal in a bridging bidentate manner as has been observed in case of previously reported poly(acrylate) supported peroxidometal complexes [21a,38a]. Three numbers of side-on bound peroxido ligands complete the eight-fold co-ordination around each Ta(V) centre. The structure envisaged for the compound **PSSTa**, shows an eight co-ordinated Ta(V) with two unidentate sulfonate moieties and three η^2 peroxido groups in the co-ordination sphere.

2. CATALYTIC ACTIVITY STUDY:

2.1 Catalytic activity of heterogeneous complex, ChpV

Oxidation of sulfides to sulfoxides

We have explored the catalytic performance of the chitosan immobilized pV compound, **ChpV** as heterogeneous catalyst in selective oxidation of organic sulfides to sulfoxide using 30% H_2O_2 as terminal oxidant, under variety of reaction conditions. In order to optimize the reaction condition to achieve best conversion and selectivity, the influence of key factors such as type of solvent, substrate: H_2O_2 stoichiometry, catalyst concentration etc., were investigated using methyl phenyl sulfide as representative substrate. The details of the study are shown in **Table 7**.

Effect of concentration of oxidant

In an exploratory experiment, the reaction of MPS with H_2O_2 , maintaining molar ratio of MPS: H_2O_2 at 1:2 and catalyst: substrate ratio at 1:1000, was conducted in aqueous medium at ambient temperature under magnetic stirring. As evident from the data presented in **Table 4** (entry 1), under these conditions MPS was completely transformed in to sulfoxide with 100% selectivity. The TOF could be improved further by increasing the amount of oxidant gradually from 2 to 5 equivalents. More than 10-fold rise in TOF (**Table 7**, entry 4) could be achieved with 5 equivalents of H_2O_2 , without affecting the selectivity of the reaction. Interestingly, further increase in the oxidant amount to 6 equivalents led to over oxidation of sulfoxide to sulfone

rendering the reaction non-selective, although a substantial increase in TOF occurred (**Table 7**, entry 5).

Effect of catalyst amount

Apart from the oxidant concentration, the amount of catalyst was observed to have a significant influence on the rate and selectivity of the sulfide oxidation. As illustrated in **Table 4**(entry 6), the catalyst was found to be effective even at V: substrate molar ratio of 1:2000 affording a reasonably good TOF. Increase in the catalyst amount **Table 7** (entry 7) although accelerated the process as expected, however, the reaction resulted in a reduced TOF and partial over oxidation of sulfoxide to sulfone. Thus for achieving high conversion without compromising the sulfoxide selectivity in aqueous medium, catalyst: substrate molar ratio of 1:1000 and substrate: oxidant ratio of 1: 5 have emerged to be optimal.

The importance and role of the catalyst in facilitating the formation of the target product was confirmed by conducting a control experiment in absence of the catalyst. The reaction under such condition was found to be rather slow and non-selective leading to the formation of both sulfoxide and sulfone in <12% yield (**Table 7**, entries 16,17) within the stipulated reaction time. With an aim to compare the activity of the heterogeneous pV catalyst with the homogeneous one, we have conducted the oxidation reaction using a previously reported water soluble monomeric diperoxidovanadate complex, $K[VO(O_2)_2(H_2O)]$ (DPV) [51], in lieu of the heterogeneous pV catalyst, **ChpV** maintaining similar catalyst concentration (V:MPS::1:1000). As seen from the results in **Table 7** (entries 18,19), in presence of the free complex specie, $[VO(O_2)_2(H_2O)]^-$ complex species the TOF obtained was nearly half of that afforded by the polymer supported heterogeneous catalyst, **ChpV** under otherwise analogous reaction condition. Moreover, DPV catalyzed reaction provided a mixture of sulfoxide and sulfone and hence was found to be less selective.

Effect of solvent

We have also screened the performance of the catalyst in common organic solvents, in addition to water. In order to assess the solvent effect we have chosen relatively safer organic solvents such as methanol, ethanol and acetonitrile in the oxidation of MPS [52]. It is pertinent to mention that in the present study, we have strategically avoided the use of hazardous chlorinated solvents. To our pleasure, as seen from the data depicted in **Table 7**, the catalytic protocol for sulfoxidation was observed to be compatible with each of the tested organic solvents. In fact, the catalyst turned out to be more potent in organic solvents compared to water, providing best results in acetonitrile with respect to both product selectivity and TOF even with 1 equivalent of H_2O_2 (**Table 7**, entry 8). This may not be surprising in view of the complete solubility of the organic substrate in these solvents. Nearly 4-fold improvement in the TOF could be achieved in acetonitrile simply by increasing the amount of oxidant to 2 equivalents maintaining the catalyst: substrate ratio as 1:1000 (**Table 7**, entry 9). Further increase in amount of oxidant however, led to loss of selectivity of the reaction (**Table 7**, entry 10). Thus, in acetonitrile a substrate: oxidant molar ratio of 1: 2 was found to be optimal (**Table 7**, entry 9). Moreover, as can be seen from the

results presented in **Table 7** (entry 9), the catalyst: substrate ratio of 1: 1000 proved to be conducive to attain best conversion in acetonitrile also. It is thus remarkable that the same catalyst enabled us to achieve selective oxidation of sulfides in aqueous medium as well as in organic solvent by a versatile variation of reaction condition, as shown in **Table 7**.

Subsequently, we have extended the study to a range of structurally diverse sulfides such as dialkyl, diaryl, aryl alkyl, aryl allyl, aryl alcohol etc. in experiments conducted independently in water as well as acetonitrile under the respective standardized reaction conditions. The results depicted in **Tables 8** and **9**, demonstrated that excellent yield with complete selectivity was possible to be attained with the series of substrates examined in presence of the catalyst. Importantly, no over oxidation of sulfoxide to sulfone was observed in any of the tested substrates under the investigated condition.

That the nature of the substituent influenced the rate of oxidation was evident from the variations in the TOF values within the substrates examined. Dialkyl sulfides were oxidized by H_2O_2 at a faster rate with higher TOF compared to allylic sulfides. In fact, dimethyl sulfide was oxidized with the highest TOF of 5628 and 5688 h^{-1} in water and acetonitrile, respectively (**Table 8**, entry 2 and **Table 9**, entry 2). On the other hand, in case of conjugated system such as diphenylsulfide, the reaction was found to be rather sluggish with a relatively poor TOF (**Table 8**, entry 9 and **Table 9**, entry 9). The observed trend in rates of oxidation is in accord with the decreasing nucleophilicity of the thioethers examined.

An additional attractive feature of the methodology, irrespective of the solvent used, is the excellent chemoselectivity of the catalyst towards sulphur group of substituted sulfides with other oxidation prone functional groups. Thus allylic and alcoholic sulfoxides were obtained without affecting any other functional group transformation (**Table 8**, entries 7,8 and **Table 9**, entries 7,8). The protocol for sulfide oxidation was also applied for high scale synthesis of sulfoxide up to ten fold under optimized condition (**Table 8**, entry 1^c and **Table 9**, entry 1^c). The H_2O_2 efficiency in the oxidation reaction under optimized condition was found to be greater than 90% for all substrates except for diphenyl sulfide (67% in H_2O and 73% in CH_3CN) complementing the higher activity of the catalyst within reasonably short reaction time in both CH_3CN and H_2O . The efficiency was measured as $100 \times$ moles of H_2O_2 consumed in the formation of oxyfunctionalized products per mole of H_2O_2 converted [53].

Test for heterogeneity of the reaction

To confirm the heterogeneity of the reaction, separate experiments were carried out by using MPS as substrate under standard protocol. After completion of the reaction, the solid catalyst was separated by filtration and the filtrate was treated with fresh batch of MPS and 30% H_2O_2 . The reaction was allowed to continue for another 1h. It was found that the conversion was very low, only about 11% in H_2O (9% in CH_3CN) which is close to the conversion obtained from control experiment conducted in absence of the catalyst (**Table 7**, entries 16,17). That the reaction did not proceed on removal of the catalyst was thus evident. Moreover, absence of vanadium in the filtrate obtained after separating the solid catalyst was ascertained by ICP-OES

analysis. These observations refute the possibility of leaching of metal complex from the polymer incorporated catalyst into the reaction medium during the oxidation reaction, which further proves the heterogeneity of the catalytic process.

Recyclability of the catalyst

Owing to the heterogeneous nature of the catalyst, it could be easily separated from the spent reaction mixture and recharged in the subsequent reaction run. The recyclability of the catalyst was tested for five reaction cycles using MPS as the substrate. Recycling experiments were performed by charging the spent catalyst with a fresh batch of substrate, H₂O₂ and the respective solvent (CH₃CN or H₂O) after completion of each reaction cycle. The catalyst could be reused at least up to five reaction cycles with consistent activity and selectivity when acetonitrile was used as solvent (**Table 9** and **Fig. 24**). The FT-IR spectrum of the spent catalyst showed the characteristic bands corresponding to chitosan and metal-peroxido stretching as has been observed in the spectrum of original catalyst. Moreover, no significant decrease in vanadium content value of the recovered catalyst was indicated by the ICP-OES analysis and EDX spectral data compared to the starting catalyst. In case of the reaction conducted in water, the catalyst could be reused with consistent activity and selectivity up to 3rd cycle, after which a slight decrease in activity was noted indicating a small amount of leaching of pV species (**Table 8** and **Fig. 24**).

2.2 Catalytic activity of homogeneous complex, PAmV

In case of oxidation, the reaction parameters including type of solvent, H₂O₂ concentration and catalyst amount were optimized for the homogeneous catalyst system, **PAmV** by taking MPS as the representative substrate. We have performed the reaction using a number of different solvents and the solvent effect on the reaction outcome is evident from the data presented in **Table 10** (entries 2-5). Although the catalyst is insoluble in neat organic solvent, but in presence of H₂O₂, the catalyst dissolved completely in water miscible solvents which provided homogeneity to the reaction process. Methanol was found to be the most suitable solvent for achieving complete conversion of sulfide with 100% sulfoxide selectivity in a reaction conducted at room temperature, maintaining a catalyst:substrate molar ratio of 1:1000 with 2 equivalents of 30% H₂O₂ (**Table 10**, entry 2). Increasing the H₂O₂ concentration to three equivalents led to a significant rate enhancement, but selectivity was compromised with formation of both sulfoxide and sulfone (**Table 10**, entry 6). Thus a substrate:oxidant ratio of 1:2 was found to be most conducive to attain complete conversion to sulfoxide as the sole product. An assessment of effect of the different catalyst amounts on rate of oxidation as illustrated in **Table 10** (entries 7,8) revealed that catalyst:substrate ratio of 1:1000 provided the best results in terms of rate as well as selectivity.

Under the standardized reaction condition, a blank reaction conducted in absence of the catalyst afforded only 6% of conversion with poor selectivity. Similarly, the reaction conducted

in presence of unsupported pV catalyst Na[VO(O₂)₂] as shown in **Table 10** (entry 9) was found to be non-selective. These observations demonstrate the importance of the immobilized catalyst **PAmV** in facilitating the reaction under investigation.

The wider applicability of the developed methodology was explored using a number of structurally variant sulfides and the findings are summarized in **Table 11**. Each of the substrates was selectively transformed into the respective pure sulfoxide with impressive yield and TOF in presence of the catalyst. As expected on the basis of their difference in nucleophilicity, aliphatic sulfides were oxidized at a faster rate compared to aromatic sulfides and also other functionalized sulfides *viz.* allylic and alcoholic sulfides. The catalyst displayed complete chemoselectivity towards sulfur group of substituted sulfides with co-existing functional groups susceptible to oxidation [**Tables 11** (entries 6,7)].

Soluble catalysts are often associated with limitations with respect to difficulty in their regeneration owing to their homogeneous nature. In the present study, the catalyst was regenerated *in situ* after the separation of the organic products from the reaction mixture by extracting it with diethyl ether, after complete conversion of the substrates. It was found that the catalyst was able to regenerate till third cycle without any significant loss in activity and selectivity, as seen in **Table 11** (entry 1^a).

3. INVESTIGATION OF BIOCHEMICAL ACTIVITY OF THE COMPOUNDS

In the present investigation, we have carried out study on kinetics of *in vitro* inhibition of activity of wheat thylakoid membrane acid phosphatase (ACP) by pV and pTa compounds in analogous macroligand environment, [V₂O₂(O₂)₄(carboxylate)]-PA (**PAV**) [24a], [VO(O₂)₂(sulfonate)]-PSS (**PSSV**) [21a], and [Ta(O₂)₃(carboxylate)]-PA (**PATa**) [54] and [Ta(O₂)₃(sulfonate)₂]-PSS (**PSSTa**) [54] as well as their respective neat monomeric precursor complexes, Na[VO(O₂)₂(H₂O)] (**DPV**) [51] and tetraperoxidotantalate Na₃[Ta(O₂)₄]·H₂O (**TpTa**) [25a]. We endeavoured to draw comparison between the two types of peroxidometallates, polymer bound as well as free, with respect to their tested properties. The findings of our investigation on the stability of the pTa compounds, homoleptic tetraperoxidotantalate Na₃[Ta(O₂)₄]·H₂O (**TpTa**) [25a] and macrocomplexes **PATa** and **PSSTa** [54] are also reported herein.

3.1 Stability of the compounds toward decomposition in solution

Since the objective of the present study was to explore the biological attributes of pTa compounds, we considered it necessary to ascertain the stability of these newly synthesized pTa compounds towards degradation in aqueous solution under different pH conditions since all the compounds are soluble in water. The stability of the pTa compounds was investigated at natural pH attained by dissolving the compounds in water.

Moreover, stability of the compounds was assessed under a wide range of pH value ranging from acidic to high pH (**Fig. 25**). The studies revealed that the peroxide content of all the tested peroxidotantalum compounds comprising of monomeric tetraperoxidotantalate, **TpTa** and polymer anchored pTa compounds **PATa** and **PSSTa**, remained practically same even after a period of 12 h. The observation indicated the stability of the compounds in aqueous solution under a wide range of pH values such as 1.2, 2.1, 3.1, 4.6, 7.0 and 8.0. Furthermore, ^{13}C NMR spectra of the compounds did not show any change in the spectral pattern when monitored over a period of 12 h. From these evidences, it has been confirmed that the immobilized pTa compounds, **PATa** and **PSSTa** retain their structural integrity and remain stable in solution under the tested reaction conditions. The title pV compounds *viz.* **PAV** and **PSSV** have already been reported to be stable in solution within a pH range of 3.6-8.0 over a period of 12 h [21a,24a]. Thus, the observed stability of the compounds encouraged us to further explore their biochemical attributes.

3.2 Interaction of pTa compounds with catalase

Catalase is an enzyme that catalyzes disproportionation of H_2O_2 into water and molecular oxygen. Being a reactive oxygen species, hydrogen peroxide has long been known as a metabolic toxic waste product, responsible for DNA damage, oxidative degradation of proteins and lipids which ultimately lead to cell death [55]. During the last two decades, several groups have enormously contributed in changing the notion and documented the significance of H_2O_2 as a key signal transducing agent modulating a variety of cellular processes [56]. However, its rapid decomposition in presence of ‘intracellular detoxifier’ catalase and glutathione peroxidase has been the major caveat for studying its multiple cellular effects [56a-d]. Therefore, there have been efforts to find more stable peroxide derivatives that are less susceptible to degradation by peroxide scavenging enzymes, which would effectively substitute H_2O_2 at much lower concentration and replicate their actions. Previous studies have demonstrated that diperoxidovanadate (**DPV**) being nearly 50 times more stable to catalase *vis-a-vis* hydrogen peroxide [21a,57], can substitute H_2O_2 in myriads of biological activities *viz.*, insulin-mimetic actions, cell proliferation, smooth muscle contraction, and also modulation of various signalling events [56c,d,57]. Subsequently, we have observed that the macro complexes **PAV** and **PSSV**, obtained by anchoring of **DPV** to WSP support, displayed even greater resistance to catalase compared to **DPV**, as revealed by their slower rates of peroxide loss under the effect of catalase [21a]. It is pertinent to mention that like pV compounds, several of our synthesized pMo [21a], pW [58] as well as pNb [3b] compounds were reported to display slower rates of degradation in presence of catalase, while there are no available reports on the interaction of discrete pTa compounds with catalase.

The effect of catalase action on the newly synthesized polymer anchored pTa compounds as well as the precursor complex, **TpTa** are shown in **Fig. 25**. Excellent ability of the pTa compounds to withstand catalase action is evident from rates of peroxide loss from the compounds, ranging between 0.92 to 2.54 $\mu\text{M}/\text{min}$ (**Table 4**, entries 1-3). These rates are *ca.* 5-6 times slower relative to the corresponding V containing analogues [21a] with similar ligand environment under same reaction conditions (**Table 4**). The trend observed for the title compounds is in the following order of increasing stability towards catalase: **PATa** > **PSSTa** > **TpTa**. Interestingly, a similar trend with respect to catalase resistance ability has also been displayed by the pV analogues which could be arranged as **PAV** > **PSSV** > **DPV**. Thus, the free monomeric DPV as well as **TpTa** complexes are at least 50% less resistant to catalase action as revealed by their higher rates of peroxide loss relative to the respective polymer immobilized counterparts. These observations clearly demonstrate that immobilization of peroxidometallates on polymer support imparts additional stability to the complexes. The extraordinary stability of the pTa compounds is further revealed by the loss of only one peroxido group from the triperoxidoTa species of the complexes, **PATa** and **PSSTa** in presence of catalase, even after extending the reaction time up to 1 h, resulting in the formation of a stable diperoxidoTa(V) in presence of catalase as seen in **Fig. 25**. Interestingly, formation of a diperoxidoTa(V) was also indicated in case of the neat tetraperoxido complex, **TpTa** by the loss of two peroxido groups under the effect of catalase. It is noteworthy that addition of catalase to peroxido compounds of V, Mo, and W resulted in complete loss of peroxido group within *ca.* 30 min of incubation [21a,39,58], while pNb compounds showed unique feature of retaining one peroxido group beyond a period of 1 h [3b]. In the present study, pTa compounds displayed a degradation pattern similar to peroxidoniobium complexes by retaining one of the peroxido groups even beyond 4 h.

According to previous report, addition of catalase to 0.1 mM solution of H_2O_2 resulted in rapid degradation at a rate of 430 $\mu\text{M}/\text{min}$ which led to its complete decomposition within *ca.* 2 min of reaction time [57]. On comparing this value to the rate of peroxide loss from the synthesized pTa compounds, it has been observed that pTa compounds are nearly 200-400 times weaker as substrates to catalase compared to its native substrate, H_2O_2 . Thus, these pTa complexes have emerged as the most resistant species towards catalase action among the synthetic peroxidometallate systems investigated so far.

3.3 Effect of pV and pTa complexes on the activity of acid phosphatase

The *in vitro* effect of the pV containing macro complexes **PAV**, **PSSV** (**Fig. 26**) and their Ta containing analogues **PATa** and **PSSTa** (**Fig. 23**) as well as free homoleptic complexes of the two metals *viz.*, **DPV** (**Fig. 26**) and **TpTa**, on the activity of ACP was investigated by employing an established assay system and with *p*-NPP as substrate [3b-

d,58a,59]. The dose dependent inhibition of the model enzyme by the tested complexes is depicted in **Fig. 27**. It is evident that with increasing inhibitor concentration the % ACP activity gradually decreases in presence of each of the tested species. The inhibitory potential of each of the tested compounds was determined quantitatively from these plots by measuring the half maximal inhibitory concentration (IC_{50}). The IC_{50} values, which represent 50% suppression of the actual enzyme activity, are presented in **Table 13**. The IC_{50} values for pTa compounds were recorded to be in the range of 0.3-5.1 μ M, while for pV compounds it was in the range of 1-17 μ M. These data demonstrate that, each of the tested pV and pTa complexes actively inhibit ACP function even at very low compound concentration. However, the IC_{50} values clearly show that, peroxidotantalum complexes are 2-3 fold more potent inhibitors compared to the respective pV analogues.

On comparing the IC_{50} values of the pV macro complexes with the monomeric **DPV** (**Table 13**, entries 4-6), the compounds could be arranged in the following order of potency- **PSSV** > **PAV** > **DPV**, whereas pTa complexes showed the following trend: **PSSTa** > **TpTa** > **PATa**. The relatively higher inhibitor efficiency displayed by the free monomeric **TpTa**, may possibly be correlated to the presence of four η^2 -peroxido ligands in the co-ordination sphere of this holmoleptic tetraperoxidotantalate complex. Moreover, in case of **TpTa** (**Fig. 27b**), after the initial suppression of ACP activity to *ca.* 60% with 1.0 μ M concentration of the inhibitor, an abrupt decrease in ACP activity was noted on further increase of the **TpTa** concentration to 1.5 μ M, resulting in non-linearity of the plot. The exact cause of this observation is however not clear at this stage. An interesting common feature revealed by these trends is the remarkable inhibitor efficiency displayed by the macro complexes **PSSV** and **PSSTa** bound to the polymer PSS. In fact, **PSSTa** has been found to be the most potent inhibitor with its sub-micromolar IC_{50} value as low as 0.34 μ M. The observation is consistent with previous findings from our laboratory showing PSS anchored peroxidoniobium and peroxidotungsten complexes as the most effective inhibitors of ACP [3c,58a,60]. Since individually neither the pristine polymers nor H_2O_2 had any observable effect on ACP function, it can safely be inferred that the inhibitor activity of the test compounds originates from the interaction of the intact metal complexes with the enzyme. It is also evident from these observations that the nature of the co-ligand environment affects the inhibitory ability of the tested species substantially.

3.4 Kinetics of ACP inhibition by pV and pTa compounds

Enzyme kinetics investigation is a major implement for distinguishing between different modes of inhibition of enzyme catalyzed reactions such as competitive, non-competitive or mixed type of inhibition. Therefore, in order to elucidate the mode of the observed inhibitory effect displayed by the pV and pTa complexes, the steady state kinetics of the ACP catalyzed hydrolysis of *p*-NPP was investigated. The kinetic parameters, K_m and V_{max} were determined from the Lineweaver-Burk double reciprocal

plots^{43b,44} where the reciprocal initial velocity was plotted against the reciprocal substrate concentration in absence or presence of the inhibitor species at different concentrations, as shown in **Fig. 28-29**. The kinetic measurements for the pV and pTa compounds including free monomeric (**DPV** and **TpTa**) as well as polymer anchored compounds (**PAV**, **PSSV**, **PATa** and **PSSTa**), produced straight lines which intercepted at a point in close proximity to the $1/[S]$ axis. From these plots it is evident that with increasing concentration of the inhibitor species, the value of velocity V_{\max} decreased, whereas K_m value remained constant. This suggested non-competitive mode of inhibition for each of the tested inhibitor species.

To ascertain the affinity of the enzyme for the inhibitor species, we have also determined the inhibitor constants, K_i and K_{ii} . The inhibitor constant, K_i is the measure of inhibitor's affinity to the free enzyme which was obtained from the x-intercepts of the secondary plot of the slope of the primary L-B plot *versus* the inhibitor concentration, shown in **Fig. 28-29** [inset (a)]. Whereas, the constant K_{ii} reveals inhibitor's affinity for the enzyme-substrate complex, determined from the re-plot of the intercepts of the primary L-B plot against the inhibitor concentration with x-intercept of this graph being equivalent to K_{ii} [**Fig. 28-29**, inset (b)]. The values of K_i and K_{ii} for each of the inhibitor species are listed in **Table 13**. The inhibitory constant for the competitive part of inhibition, K_i values for the tested inhibitor compounds was found to be comparable to the inhibitor constant for the non-competitive part of inhibition, K_{ii} with the ratio of K_{ii}/K_i values being close to unity. These observations are typical of a non-competitive inhibitor and are in accord with the mechanism of inhibition displayed by other polymer bound peroxidometallates reported previously from our laboratory [3b,c,21a,58a,60]. The trend in inhibition potency of the pV and pTa compounds revealed by the kinetic measurements (**Table 13**) has been found to be consistent with that obtained from their IC_{50} values.

A non-competitive inhibitor usually binds to the enzyme reversibly at a site far removed from the active site which causes alteration in the overall three dimensional shape of the enzyme leading to reduced activity of the enzyme [3b,c]. The non-competitive inhibitor has the same affinity for both the enzyme and enzyme-substrate complex. Phosphatases, in general, are known to be inhibited by smaller oxyanions of V, Mo and W with penta or hexa co-ordinated structures in a competitive manner, as these ions share structural analogy with phosphate [3b,c,21a,61]. However, in case of acid phosphatases, different oxidometal ions inhibited the ACP function *via* diverse pathways ranging from competitive, non-competitive to uncompetitive modes [3b,c,61a-c,62]. For example, Fei *et al.*[3a] reported molybdate and vanadate to be un-competitive and non-competitive inhibitor of wheat thylakoid acid phosphatase, respectively whereas, Das *et al.*[3c] also observed non-competitive mode of inhibition on ACP by tungstate. Averill and his co-workers reported tungstate and molybdate as non-competitive inhibitor of bovine spleen purple acid phosphatase [63]. These information suggested different mechanistic preferences for different oxidometal ions in inhibition of acid phosphatase, in

spite of having similar structural characteristics. It is however notable that, reports pertaining to ACP inhibition by peroxidometallates are still very scarce, in spite of the extensive studies on peroxidovanadate systems in inhibition of phosphohydrolases.

Acid phosphatase, isolated from various sources *viz.* human prostate, wheat germ, plant possesses dinuclear iron at active site with histidine residue and highly conserved amino acid sequence [3a,62-64]. It is relevant to recall here the work of Averill and his co-workers, wherein oxyanions such as molybdate and tungstate, presumably because of their larger size, induce non-competitive inhibition of bovine spleen purple acid phosphatase by binding the two iron atoms in the binuclear active site of the enzyme in a bridging manner [63]. The peroxidometal derivatives examined in the present study possibly inhibits the ACP function in a non-competitive manner as they are unlikely to bind to the enzyme active site as transition state analogue, due to their larger size, ^{9b-e} Additionally, as has been demonstrated by Fei *et al.*, the enzyme could be inactivated by the highly oxidative species *via* oxidative transformation of the Fe²⁺ centre in the active site of the enzyme to its ferric form resulting in non-competitive inhibition of the enzyme [3a]. According to previous literature, peroxidovanadate exerted inhibitory effect on tyrosine phosphatase by oxidizing the cysteine residue in the catalytic domain of the enzyme [65]. Taking into account these important findings, the observed non-competitive inhibition by the pV and pTa compounds in the present study may safely be attributed to their oxidative interaction with either Fe²⁺ centre in the active site or oxidation prone –SH groups of the protein chain. Such groups play crucial role in stabilization of the quaternary structure and are essential for enzyme activity [3a,c]. It is reasonable to expect redox interaction between the inhibitor complexes and the enzyme as the compounds examined herein, were also found to actively facilitated oxidation of organic substrates [24a,66]. However, in absence of direct evidence and considering the complexity of involved biological process, it is somewhat difficult to draw any definite conclusion regarding exact mechanism of inhibition by the tested compounds. Further investigation in this respect will evidently be necessary to unravel the actual mechanism of observed inhibition. Nevertheless, existence of substantial reports on phosphatase inhibitory ability of pV compounds offer adequate credibility to our proposed hypothesis.

Reference:

1. M. K. Chaudhuri, S. K. Ghosh, N. S. Islam, *Inorg. Chem.*, 1985, **24**, 2706.
2. (a) S. R. Gogoi, J. J. Boruah, G. Sengupta, G. Saikia, K. Ahmed, K. K. Bania, N. S. Islam, *Catal. Sci. Technol.*, 2015, **5**, 595. (b) J. J. Boruah, S. P. Das, S. R. Ankireddy, S. R. Gogoi, N. S. Islam, *Green Chem.*, 2013, **15**, 2944.
3. (a) M. J. Fei, J. S. Chen and X. Y. Wang, *Journal of Integrative Plant Biology*, 2006, **48**(3), 294. (b) S. R. Gogoi, G. Saikia, K. Ahmed, R. Duarah and N. S. Islam, *Polyhedron*, 2017, **121**, 142. (c) S. P. Das, S. R. Ankireddy, J. J. Boruah and N. S. Islam, *RSC Advances*, 2012, **2**(18), 7248. (d) H. U. Bergmeyer, J. Bergmeyer and M. Grassl, *Methods of Enzymatic Analysis*. Verlag Chemie, Weinheim, Deerfield Beach, 3rd edition, 1983.
4. C. V. Ferreira, E. M. Taga and H. Aoyama, *Plant Science*, 1999, 147(1), 49.
5. (a) H. Lineweaver and D. Burk, *Journal of the American Chemical Society*, 1934, **56**(3), 658. (b) A. Cornish-Bowden, *Perspectives in Science*, 2014, **1**(1), 74.
6. (a) K. D. Trimukhe and A. J. Varma, *Carbohydrate Polymers*, 2008, **71**(1), 66. (b) A. Webster, M. D. Halling and D. M. Grant, *Carbohydrate Research*, 2007, **342**(9), 1189. (c) S. R. Acharyulu, T. Gomathi and P. N. Sudha, *Der Pharmacia Lettre*, 2013, **5**(2), 354.
7. (a) X. Wang, Y. Du and H. Liu, *Carbohydrate Polymers*, 2004, **56**(1), 21. (b) C. Ou, S. Li, J. Shao, T. Fu, Y. Liu, W. Fan, X. Yang and X. Bi, *Cogent Chemistry*, 2016, **2**(1), 1216247. (c) X. Wang, Y. Du, L. Fan, H. Liu and Y. Hu, *Polymer Bulletin*, 2005, 55(1-2), 105. (d) C. Y. Ou, C. H. Zhang, S. D. Li, L. Yang, J. J. Dong, X. L. Mo and M. T. Zeng, *Carbohydrate Polymers*, 2010, **82**, 1284.
8. (a) M. M. AbdElhady, *International Journal of Carbohydrate Chemistry*, 2012, 1. (b) M. H. M. Hussein, M. F. El-Hady, W. M. Sayed and H. Hefni, *Polymer Science Series A*, 2012, **54**(2), 113. (c) R. Ramya, P. N. Sudha and J. Mahalakshmi, *International Journal of Scientific and Research Publications*, 2012, **2**(10), 1.
9. (a) M. Occhiuzzi, S. Tuti, D. Cordischi, R. Dragone and V. Indovina, *Journal of the Chemical Society, Faraday Transactions*, 1996, **92**(21), 4337. (b) B. Horvath, J. Strutz, J. Geyer-Lippmann and E. G. Horvath, *Zeitschrift für Anorganische und Allgemeine Chemie*, 1981, **483**(12), 181. (c) M. Faraldos, J. A. Anderson, M. A. Banares, J. L. G. Fierro and S. W. Weller, *Journal of Catalysis*, 1997, **168**(1), 110. (d) R. K. Jha, S. Shylesh, S. S. Bhoware and A. P. Singh, *Microporous and Mesoporous Materials*, 2006, **95**(1-3), 154. (e) J. Mendialdua, R. Casanova and Y. Barboux, *Journal of Electron Spectroscopy and Related Phenomena*, 1995, **71**(3), 249. (f) Y. Zhang, C. Chen, W. Wu, F. Niu, X. Liu, Y. Zhong, Y. Cao, X. Liu and C. Huang, *Ceramics International*, 2013, **39**(1), 129. (g) M. C. Biesinger, L. W. Lau, A. R. Gerson and R. S. C. Smart, *Applied Surface Science*, 2010, **257**(3), 887.
10. (a) M. Kantcheva, *Physical Chemistry Chemical Physics*, 2000, 2(13), 3043. (b) E. Mikolajska, V. Calvino-Casilda and M. A. Bañares, *Applied Catalysis A: General*, 2012, **421**, 164. (c) E. P. Reddy, L. Davydov and P. G. Smirniotis, *The Journal of Physical Chemistry B*, 2002, **106**(13), 3394.
11. (a) S. Brunauer, P. H. Emmett and E. Teller, *Journal of the American Chemical Society*, 1938, **60**(2), 309. (b) E. P. Barrett, L. G. Joyner and P. P. Halenda, *Journal of the American Chemical Society*, 1951, **73**(1), 373.
12. (a) K. S. Sing, D. H. Everett, R. A. W. Haul, L. Moscou, R. A. Pierotti, J. Rouquerol and T. Siemieniewska, *Pure Applied Chemistry*, 1985, **57**(4), 603. (b) S. J. Gregg and K. S. W. Sing, *Adsorption, Surface Area and Porosity*. Academic Press, London, 1982. (c) M. Thommes, K. Kaneko, A. V. Neimark, J. P. Olivier, F. Rodriguez-Reinoso, J. Rouquerol and K. S. Sing, *Pure and Applied Chemistry*, 2015, **87**(9-10), 1051. (d) M. Lawrence and Y. Jiang, Porosity, pore size distribution, micro-structure. In *Bio-aggregates Based Building Materials*, pages 39-71. Springer, Dordrecht, 2017.
13. K. A. Alkhamis, M. S. Salem and M. S. Khanfar, *Aaps Pharmscitech*, 2008, **9**(3), 866.
14. X. Fei Liu, Y. Lin Guan, D. Zhi Yang, Z. Li and K. De Yao, *Journal of Applied Polymer Science*, 2001, **79**(7), 1324.
15. (a) O. Pornsunthorntawee, C. Katepetch, C. Vanichvattanadecha, N. Saito and R. Rujiravanit, *Carbohydrate Polymers*, 2014, **102**, 504. (b) M. A. Ali, S. Srivastava, K. Mondal, P. M. Chavhan, V. V. Agrawal, R. John, A. Sharma and B. D. Malhotra, *Nanoscale*, 2014, **6**(22), 13958. (c) I. K. D. Dimzon and T. P. Knepper, *International Journal of Biological Macromolecules*, 2015, **72**, 939.
16. (a) P. Hazarika, D. Kalita, S. Sarmah, R. Borah and N. S. Islam, *Polyhedron*, 2006, **25**(18), 3501. (b) Y. Feng, A. Schmidt and R. A. Weiss, *Macromolecules*, 1996, **29**(11), 3909. (c) M. K. Nagata, P. S. Brauchle, S. Wang, S. K. Briggs, Y. S. Hong, D. W. Laorenza, A. G. Lee and T. D. Westmoreland, *Polyhedron*, 2016, **114**, 299. (d) H. Sigel, and R. B. Martin, *Chemical Reviews*, 1982, **82**(4), 385.
17. (a) A. J. Varma, S. V. Deshpande and J. F. Kennedy, *Carbohydrate Polymers*, 2004, **55**(1), 77. (b) S. Mekahlia and B. Bouzid, *Physics Procedia*, 2009, **2**(3), 1045.

18. (a) S. Rashid, C. Shen, J. Yang, J. Liu and J. Li, *Journal of Environmental Sciences*, 2018, **66**, 301. (b) J. Coates, Interpretation of infrared spectra, a practical approach. In *Encyclopedia of Analytical Chemistry*. John Wiley & sons, New York, 2000.
19. L. G. Tang, and D. N. S. Hon, *Journal of Applied Polymer Science*, 2001, **79**(8), 1476.
20. (a) H. Dweik, W. Sultan, M. Sowwan and S. Makharza, *International Journal of Polymeric Materials*, 2008, **57**(3), 228. (b) A. M. Dumitrescu, G. Lisa, A. R. Iordan, F. Tudorache, I. Petrila, A. I. Borhan, M. N. Palamaru, C. Mihailechu, L. Leontie, and C. Munteanu, *Materials Chemistry and Physics*, 2015, **156**, 170. (c) L. Xu, L. Che, J. Zheng, G. Huang, X. Wu, P. Chen, L. Zhang and Q. Hu, *RSC Advances*, 2014, **4**(63), 33269. (d) L. T. Chiem, L. Huynh, J. Ralston and D. A. Beattie, *Journal of Colloid and Interface Science*, 2006, **297**(1), 54.
21. (a) J. J. Boruah, D. Kalita, S. P. Das, S. Paul and N. S. Islam, *Inorganic Chemistry*, 2011, **50**(17), 8046. (b) Y. Feng, A. Schmidt and R. A. Weiss, *Macromolecules*, 1996, **29**(11), 3909. (c) W. E. Bull, S. K. Madan and J. E. Willis, *Inorganic Chemistry*, 1963, **2**(2), 303.
22. J. Zhao and J. Wang, *The Journal of Physical Chemistry B*, 2016, **120**(36), 9590.
23. K. B. Girma, V. Lorenz, S. Blaurock and F. T. Edelmann, *Coordination Chemistry Reviews*, 2005, **249**(11-12), 1283.
24. (a) D. Kalita, S. Sarmah, S. P. Das, D. Baishya, A. Patowary, S. Baruah and N. S. Islam, *Reactive and Functional Polymers*, 2008, **68**(4), 876. (b) N. J. Campbell, A. C. Dengel and W.P. Griffith, *Polyhedron*, 1989, **8**(11), 1379. (c) A. B. P. Lever and H. B. Gray, *Accounts of Chemical Research*, 1978, **11**(9), 348.
25. (a) D. Bayot and M. Devillers, *Coordination Chemistry Reviews*, 2006, **250**(19-20), 2610. (b) D. Bayot, M. Devillers and D. Peeters, *European Journal of Inorganic Chemistry*, 2005, **2005**(20), 4118. (c) G. Haxhillazi and H. Haeuseler *Journal of Solid State Chemistry*, 2004, **177**(9), 3045.
26. K. Nakamoto, *Infrared and Raman spectra of inorganic and co-ordination compounds, Part B*. Wiley and Sons, New York, 1997.
27. (a) S. R. Gogoi, K. Ahmed, G. Saikia and N. S. Islam, *Journal of the Indian Chemical Society*, 2018, **95**(7), 801. (b) H. Li and C. P. Tripp, *Langmuir*, 2004, **20**(24), 10526.
28. (a) B. L. Rivas, G. V. Seguel and K. E. Geckeler, *Journal of Applied Polymer Science*, 2002, **85**(12), 2546. (b) A. Pourjavadi and H. Ghasemzadeh, *Polymer Engineering & Science*, 2007, **47**(9), 1388.
29. S. Sarmah, D. Kalita, P. Hazarika, R. Borah and N. S. Islam, *Polyhedron*, 2004, **23**(7), 1097.
30. (a) C. A. Caro, G. Cabello, E. Landaeta, J. Pérez, M. González, J. H. Zagal and L. Lillo, *Journal of Coordination Chemistry*, 2014, **67**(23-24), 4114. (b) J. Kumirska, M. Czerwicka, Z. Kaczyński, A. Bychowska, K. Brzozowski, J. Thöming and P. Stepnowski, *Marine Drugs*, 2010, **8**(5), 1567. (c) Y. Wang, A. Pitto-Barry, A. Habtemariam, I. Romero-Canelon, P. J. Sadler and N. P. Barry, *Inorganic Chemistry Frontiers*, 2016, **3**(8), 1058.
31. C. Djordjevic, N. Vuletic, M. L. Renslo, B. C. Puryear and R. Alimard, *Molecular and cellular biochemistry*, 1995, **153**(1-2), 25.
32. (a) P. J. Cordeiro and T. D. Tilley, *Langmuir*, 2011, **27**(10), 6295. (b) D. A. Ruddy and T. D. Tilley, *Journal of the American Chemical Society*, 2008, **130**(33), 11088.
33. (a) M. R. Kasaai, *Carbohydrate Polymers*, 2010, **79**(4), 801. (b) C. Q. Qin, Y. M. Du and L. Xiao, *Polymer Degradation and Stability*, 2002, **76**(2), 211. (c) E. Guibal, C. Milot, O. Eterradosi, C. Gauffier and A. Domard, *International Journal of Biological Macromolecules*, 1999, **24**, 49. (d) O. A. Monteiro Jr and C. Airoidi, *International Journal of Biological Macromolecules*, 1999, **26**(2-3), 119. (e) Z. Modrzejewska, M. Dorabalska, R. Zarzycki and A. Wojtasz-Pajak, *Progress on Chemistry and Application of Chitin and its Derivatives*, 2009, **XIV**, 49.
34. T. Wu, C. Wu, Y. Xiang, J. Huang, L. Luan, S. Chen and Y. Hu, *RSC Advances*, 2016, **6**(80), 76280.
35. F. O. Garces, K. Sivadasan, P. Somasundaran and N. J. Turro, *Macromolecules*, 1994, **27**(1), 272.
36. P. M. Angus, D. P. Fairlie and W. G. Jackson, *Inorganic Chemistry*, 1993, **32**(4), 450.
37. (a) A. Bodor, I. Bányai and I. Tóth, *Coordination Chemistry Reviews*, 2002, **228**(2):175-186, 2002. (b) L. L. Justino, M. L. Ramos, M. M. Caldeira and V. M. Gil, *Inorganica Chimica Acta*, 2000, **311**(1-2), 119.
38. (a) G. Saikia, S. R. Gogoi, J. J. Boruah, B. M. Ram, P. Begum, K. Ahmed, M. Sharma, G. Ramakrishna, T. Ramasarma and N. S. Islam, *ChemistrySelect*, 2017, **2**(21), 5838. (b) S. R. Gogoi, J. J. Boruah, G. Sengupta, G. Saikia, K. Ahmed, K. K. Bania and N. S. Islam, *Catalysis Science & Technology*, 2015, **5**(1), 595. (c) S. R. Gogoi, G. Saikia, K. Ahmed, R. Duarah and N. S. Islam, *Polyhedron*, 2017, **121**, 142.
39. P. Hazarika, S. Sarmah, D. Kalita and N. S. Islam, *Transition Metal Chemistry*, 2008, **33**(1), 69.
40. (a) V. Conte and B. Floris, *Dalton Transactions*, 2011, **40**(7), 1419. (b) C. R. Waidmann, A. G. DiPasquale and J. M. Mayer, *Inorganic Chemistry*, 2010, **49**(5), 2383. (c) C. Gabriel, M. Kaliva, J. Venetis, P. Baran, I. Rodriguez-Escudero, G. Voyiatzis, M. Zervou and A. Salifoglou, *A. Inorganic Chemistry*, 2008, **48**(2), 476. (d) A. S. Tracey

- and J. S. Jaswal, *Inorganic Chemistry*, 1993, **32**(20), 4235. (e) O. Bortolini, M. Carraro, V. Conte and S. Moro, *European Journal of Inorganic Chemistry*, 1999, **1999**(9), 1489.
41. A. S. Tracey and J. S. Jaswal, *Journal of the American Chemical Society*, 1992, **114**(10), 3835.
42. (a) C. S. Thatte, M. V. Rathnam and A. C. Pise, *Journal of Chemical Sciences*, 2014, **126**(3), 727. (b) A. Naghipour and A. Fakhri, *Environmental Chemistry Letters*, 2016, **14**(2), 207. (c) W. Liu, Y. Qin, S. Liu, R. Xing, H. Yu, X. Chen, K. Li and P. Li, *International Journal of Biological Macromolecules*, 2018, **106**, 68. (d) X. Yin, X. Zhang, Q. Lin, Y. Feng, W. Yu and Q. Zhang, *Arkivoc*, 2004, **9**:66. (e) K. Sreenivasan, *Polymer Degradation and Stability*, 1996, **52**(1), 85. (f) K. D. Trimukhe and A. J. Varma, *Carbohydrate Polymers*, 2009, **75**(1), 63. (g) E. Taboada, G. Cabrera, R. Jimenez and G. Cardenas, *Journal of Applied Polymer Science*, 2009, **114**(4), 2043.
43. J. Zawadzki and H. Kaczmarek, *Carbohydrate Polymers*, 2010, **80**(2), 394.
44. J. D. Van Dyke and K. L. Kasperski, *Journal of Polymer Science Part A: Polymer Chemistry*, 1993, **31**(7), 1807.
45. W. M. Leung, D. E. Axelson and J. D. Van Dyke, *Journal of Polymer Science Part A: Polymer Chemistry*, 1987, **25**(7), 1825.
46. H. D. Burrows, H. A. Ellis and S. I. Utah, *Polymer*, 1981, **22**(12), 1740.
47. (a) G. Aygun and R. Turan, *Thin Solid Films*, 2008, **517**(2), 994. (b) J. Capilla, J. Olivares, M. Clement, J. Sangrador, E. Iborra and A. Devos, Characterization of amorphous tantalum oxide for insulating acoustic mirrors. In *2011 Joint Conference of the IEEE International Frequency Control and the European Frequency and Time Forum (FCS) Proceedings*, pages 1-6, 2011. IEEE service centre. (c) A. Fielicke, G. Meijer and G. Von Helden, *The European Physical Journal D-Atomic, Molecular, Optical and Plasma Physics*, 2003, **24**(1), 69.
48. I. C. McNeill and S. M. T. Sadeghi, *Polymer Degradation and Stability*, 1990, **30**(2), 213.
49. D. D. Jiang, Q. Yao, M. A. McKinney and C. A. Wilkie, *Polymer Degradation and Stability*, 1999, **63**(3), 423.
50. Periasamy, A., Muruganand, S., and Palaniswamy, M. *Rasayan journal of chemistry*, 2(4):981-989, 2009.
51. S. Sarmah, P. Hazarika and N. S. Islam, *Molecular and Cellular biochemistry*, 2002, **236**(1-2), 95.
52. T. Welton, *Proc. R. Soc. A*, 2015, **471**, 1.
53. V. Hulea, A. L. Maciucu, F. Fajula, E. Dumitriu, *Appl. Catal. A*, 2006, **313**, 200.
54. G. Saikia, H. Talukdar, K. Ahmed, N. K. Gour and N. S. Islam, *New Journal of Chemistry*, 2021, **45**(29), 2848.
55. (a) S. Bhattacharjee, *Curr. Sci.*, 2005, 1113. (b) G. W. Winston, in *Stress Responses in Plants: Adaptation and Acclimation Mechanisms*, Willy-LissInc, New York, 1990, 57–86. (c) C. H. Foyer, in *Molecular Biology of Free Radical Scavenging Enzymes*, ed. J. Scandalios, Cold Spring Harbor Laboratory, New York, 1997.
56. (a) T. Ramasarma, in *Vanadium Biochemistry*, ed. M.A. Alves, Research Signpost, India, 2007, 45–76; (b) T. Ramasarma, *Proc. Indian National Sci. Acad.*, 2003, **69**, 649. (c) N. Chatterjee, S. Kiran, B. M. Ram, N. Islam, T. Ramasarma and G. Ramakrishna, *Mech. Ageing Dev.*, 2011, **132**, 230. (d) M. Giorgio, M. Trinei, E. Migliaccio and P. G. Pelicci, *Nat. Rev. Mol. Cell Biol.*, 2007, **8**, 722. (e) B. J. Goldstein, K. Mahadev and X. Wu, *Diabetes*, 2005, **54**, 311. (f) B. Chance, H. Sies and A. Boveris, *Physiol. Rev.*, 1979, **59**, 527.
57. H. N. Ravishankar, A. V. Rao and T. Ramasarma, *Arch. Biochem. Biophys.*, 1995, **321**, 477.
58. (a) S. P. Das, PhD thesis, Tezpur University, 2012. (b) P. Hazarika, D. Kalita and N. S. Islam, *J. Enzyme Inhib. Med. Chem.*, 2008, **23**, 504. (c) D. Kalita, S. P. Das and N. S. Islam, *Biol. Trace Elem. Res.*, 2009, **128**, 200. (d) P. Hazarika, D. Kalita and S. Sarmah, *Mol. Cell. Biochem.*, 2006, **284**, 39.
59. (a) M. J. Fei, J. S. Chen and X. Y. Wang, *J. Integr. Plant Biol.*, 2006, **48**, 294. (b) R. Albrecht, J. Le Petit, V. Calvert, G. Terrom and C. Périsol, *Bioresour. Technol.*, 2010, **101**, 228.
60. S. R. Gogoi, PhD thesis, Tezpur University, 2017.
61. (a) P. J. Stankiewicz and M. J. Gresser, *Biochemistry*, 1988, **27**, 206. (b) Y. S. Heo, J. M. Ryu, S. M. Park, J. H. Park, H. C. Lee, K. Y. Hwang and J. S. Kim, *Exp. Mol. Med.*, 2002, **34**, 211. (c) R. L. VanEtten, P. P. Waymack and D. M. Rehkop, *J. Am. Chem. Soc.*, 1974, **96**, 6782. (d) G. Soman, Y. C. Chang and D. J. Graves, *Biochemistry*, 1983, **22**, 4994. (e) C. C. McLauchlana, B. J. Petersb, G. R. Willsky and D. C. Crans, *Coord. Chem. Rev.*, 2015, **301**, 163.
62. D. K. Lord, N. C. Cross, M. A. Bevilacqua, S. H. Rider, P. A. Gorman, A. V. Groves, D.W. Moss, D. Sheer and T. M. Cox, *The FEBS J.*, 1990, **189**, 287.
63. J. B. Vincent, M. W. Crowder and B. A. Averill, *Biochemistry*, 1991, **30**, 3025.
64. (a) H. Bull, P. G. Murray, D. Thomas, A. M. Fraser and P. N. Nelson, *Mol. Pathol.*, 2002, **55**, 65. (b) D. F. Hunt, J. R. Yates, J. Shabanowitz, N. Z. Zhu, T. Zirino, B. A. Averill, S. T. Daurat-Larroque, J.G. Shewale, R. M. Roberts and K. Brew, *Biochem. Biophys. Res. Commun.*, 1987, **144**, 1154. (c) C. M. Ketcham, R. M. Roberts, R. C. Simmen and H. S. Nick, *J. Biol. Chem.*, 1989, **264**, 557.
65. (a) V. Khanna, M. Jain, M. K. Barthwal, D. Kalita, J. J. Boruah, S. P. Das, N. S. Islam, T. Ramasarma and M. Dikshit, *Pharmacol. Res.*, 2011, **64**, 274. (b) D. C. Crans, in *Vanadium compounds: Chemistry, biochemistry, and therapeutic applications*, ed. A. S. Tracey and D. C. Crans, Oxford University Press, UK, 1998, 82-103.

66. G. Saikia, PhD thesis, Tezpur University, 2020.

GFR 12 – A
[(See Rule 238 (1))]FORM OF UTILIZATION CERTIFICATE
FOR AUTONOMOUS BODIES OF THE GRANTEE ORGANIZATIONUTILIZATION CERTIFICATE FOR THE YEAR 2020-2021 in respect
of recurring/non-recurring
GRANTS-IN-AID/SALARIES/CREATION OF CAPITAL ASSETS

- Name of the Scheme Women Scientist Scheme A (WOS-A)
- WOS-A Reference No SR/WOS-A/CS-35/2017
- Principal Investigator Gangutri Saikia
- Whether recurring or non-recurring grants Recurring
- Grants position at the beginning of the Financial year
 - Cash in Hand/Bank -3,195.00
 - Unadjusted advances Nil
 - Total -3,195.00
- Details of grants received, expenditure incurred and closing balances: (Actuals)

Unspent Balances of Grants received years [figure as at Sl. No. 3 (iii)]	Interest Earned thereon	Interest deposited back to the Government	Grant received during the year			Total Available funds (1+2-3+4)	Expenditure incurred	Closing Balances (5-6)
			Sanction No. (i)	Date (ii)	Amount (iii)			
1	2	3	4			5	6	7
-3,195.00	Nil	Nil	SR/WO S-A/CS-35/2017	Nil	3,73,467/-	3,70,272.00	3,70,272.00	Nil

Component wise utilization of grants:

Grant-in-aid- General	Grant-in-aid- Salary	Grant-in-aid-creation of capital assets	Total
63,138.00	3,07,134.00	-	3,70,272.00

Details of grants position at the end of the year

- Cash in Hand/Bank Nil
- Unadjusted Advances
- Total Nil

Gangutri Saikia

Signature of PI

Date 15/02/2022

Signature

Name..... Chief Finance Officer

(Head of the Finance Office/With seal)

Date Tejpur University

Signature

Name..... Head of the Organisation

(With seal)

Date



Certified that I have satisfied myself that the conditions on which grants were sanctioned have been duly fulfilled/are being fulfilled and that I have exercised following checks to see that the money has been actually utilized for the purpose for which it was sanctioned:

- (i) The main accounts and other subsidiary accounts and registers (including assets registers) are maintained as prescribed in the relevant Act/Rules/Standing instructions (mention the Act/Rules) and have been duly audited by designated auditors. The figures depicted above tally with the audited figures mentioned in financial statements/accounts.
- (ii) There exist internal controls for safeguarding public funds/assets, watching outcomes and achievements of physical targets against the financial inputs, ensuring quality in asset creation etc. & the periodic evaluation of internal controls is exercised to ensure their effectiveness.
- (iii) To the best of our knowledge and belief, no transactions have been entered that are in violation of relevant Act/Rules/standing instructions and scheme guidelines.
- (iv) The responsibilities among the key functionaries for execution of the scheme have been assigned in clear terms and are not general in nature.
- (v) The benefits were extended to the intended beneficiaries and only such areas/districts were covered where the scheme was intended to operate.
- (vi) The expenditure on various components of the scheme was in the proportions authorized as per the scheme guidelines and terms and conditions of the grants-in-aid.
- (vii) It has been ensured that the physical and financial performance under W.B.B.A. DIST (name of the scheme has been according to the requirements, as prescribed in the guidelines issued by Govt. of India and the performance/targets achieved statement for the year to which the utilization of the fund resulted in outcomes given at Annexure - I duly enclosed.
- (viii) The utilization of the fund resulted in outcomes given at Annexure - II duly enclosed (to be formulated by the Ministry/Department concerned as per their requirements/specifications.)
- (ix) Details of various schemes executed by the agency through grants-in-aid received from the same Ministry or from other Ministries is enclosed at Annexure -II (to be formulated by the Ministry/Department concerned as per their requirements/specifications).

Date: 15/02/2022

Place

Tezpur

Gangulree Saikia

Signature of PI

Date 15/02/2022

Signature

Name: [Signature] Chief Finance Officer
(Head of the Finance) (With seal)

Date

Finance Officer
Tezpur University

Signature

Name: [Signature] Head of the Organisation
(With seal)

Date

Registrar
Tezpur University

(Strike out inapplicable terms)



GFR 12 – A
[(See Rule 238 (1))]

**FORM OF UTILIZATION CERTIFICATE
FOR AUTONOMOUS BODIES OF THE GRANTEE ORGANIZATION**

UTILIZATION CERTIFICATE FOR THE YEAR 2020-2021 in respect
of recurring/non-recurring
GRANTS-IN-AID/SALARIES/CREATION OF CAPITAL ASSETS

1. Name of the Scheme Women Scientist Scheme A (WOS-A)
2. WOS-A Reference No SR/WOS-A/CS-35/2017
3. Principal Investigator Gangutri Saikia
4. Whether recurring or non-recurring grants Non-recurring
5. Grants position at the beginning of the Financial year
 - (i) Cash in Hand/Bank 1,214.00
 - (ii) Unadjusted advances Nil
 - (iii) Total 1,214.00
6. Details of grants received, expenditure incurred and closing balances: (Actuals)

Unspent Balances of Grants received years [figure as at Sl. No. 3 (iii)]	Interest Earned thereon	Interest deposited back to the Government	Grant received during the year			Total Available funds (1+2-3+4)	Expenditure incurred	Closing Balances (5-6)
			Sanction No. (i)	Date (ii)	Amount (iii)			
1	2	3	4			5	6	7
1,214.00	30.00	--	SR/WO S-A/CS-35/2017	--	--	1,244.00	Nil	1,244

Component wise utilization of grants:

Grant-in-aid- General	Grant-in-aid- Salary	Grant-in-aid-creation of capital assets	Total
-	--	--	Nil

Details of grants position at the end of the year

- (i) Cash in Hand/Bank 1244.00
- (ii) Unadjusted Advances Nil
- (iii) Total 1244.00

Gangutri Saikia

Signature of PI

Date 15/02/2022

Signature

Name..... [Signature]
Chief Finance Officer
(Head of the Finance)/ (With seal)

Date Finance Officer

Tejpur University

Signature

Name..... [Signature]
Head of the Organisation

(With seal)

Date, Registrar

Tejpur University



Certified that I have satisfied myself that the conditions on which grants were sanctioned have been duly fulfilled/are being fulfilled and that I have exercised following checks to see that the money has been actually utilized for the purpose for which it was sanctioned:

- (i) The main accounts and other subsidiary accounts and registers (including assets registers) are maintained as prescribed in the relevant Act/Rules/Standing instructions (mention the Act/Rules) and have been duly audited by designated auditors. The figures depicted above tally with the audited figures mentioned in financial statements/accounts.
- (ii) There exist internal controls for safeguarding public funds/assets, watching outcomes and achievements of physical targets against the financial inputs, ensuring quality in asset creation etc. & the periodic evaluation of internal controls is exercised to ensure their effectiveness.
- (iii) To the best of our knowledge and belief, no transactions have been entered that are in violation of relevant Act/Rules/standing instructions and scheme guidelines.
- (iv) The responsibilities among the key functionaries for execution of the scheme have been assigned in clear terms and are not general in nature.
- (v) The benefits were extended to the intended beneficiaries and only such areas/districts were covered where the scheme was intended to operate.
- (vi) The expenditure on various components of the scheme was in the proportions authorized as per the scheme guidelines and terms and conditions of the grants-in-aid.
- (vii) It has been ensured that the physical and financial performance under W.O.S.A.P.S.T (name of the scheme has been according to the requirements, as prescribed in the guidelines issued by Govt. of India and the performance/targets achieved statement for the year to which the utilization of the fund resulted in outcomes given at Annexure – I duly enclosed.
- (viii) The utilization of the fund resulted in outcomes given at Annexure – II duly enclosed (to be formulated by the Ministry/Department concerned as per their requirements/specifications.)
- (ix) Details of various schemes executed by the agency through grants-in-aid received from the same Ministry or from other Ministries is enclosed at Annexure –II (to be formulated by the Ministry/Department concerned as per their requirements/specifications).

Date: 15/02/2022

Place

: Tezpur

Gangakutai Saikia

Signature of PI

Date 15/02/2022

Signature

Name..... Chief Finance Officer
(Head of the Finance)/ (With seal)

Date *Finance Officer*
Tezpur University

Signature

Name..... Head of the Organisation
(With seal)

Date *Registrar*
Tezpur University

(Strike out inapplicable terms)

STATEMENT OF EXPENDITURE

1. Sanction Order No and Date: SR/WOS-A/CS-35/2017 and 25.04.2018
2. Total Project Cost: 15,70,000/-
3. Revised Project Cost (if applicable): No
4. Date of Commencement: 15.05.2018
5. Grant received in each year:
 - a. 1st Year: 9,22,500/-
 - b. 2nd Year: NIL
 - c. 3rd Year: 3,73,467/-
 - d. Interest, if any: 1981/- (For the financial year 2018-19) + 30/- (For the financial year 2020-21)
 - e. **Total (a+b+c+d): 12,97,978/-**

STATEMENT OF EXPENDITURE

To be submitted financial year wise
(01-04-2020 to 31.03.2021)

S No (I)	Sanctioned Heads (II)	Sanctioned Cost (III)	Expenditure Incurred			Total Expenditure IV + V + VI (VII)	Balance as on (date) III - VII = (VIII)	Requirement of Funds upto 31 st March 2020	Remarks (if any)
			1 st Year (DOS to 31 st March next year) (IV)	2 nd Year (1 st April to 31 st March next year) (V)	3 rd Year & so on (1 st April to Project duration) (VI)				
1.	Fellowship	3,60,000/-	2,86,452/-	82,866/-	3,07,134/-	6,76,452/-	-3,16,452/-		
2.	Consumables	2,00,000/-	1,99,804/-	--	17,600/-	2,17,404/-	-17,404/-		
3.	Travel	15,000/-	11,797/-	--	--	11,797/-	3,203/-		
4.	Contingencies	15,000/-	15,000/-	--	6,400/-	21,400/-	-6,400/-		
5.	Others, if any	3,75,478/-	--	1,981/-	--	1,981/-	3,73,497/-		
6.	Equipment	2,50,000/-	2,48,786/-	--	--	2,48,786/-	1,214/-		
7.	Overhead expenses	82,500/-	79,776/-	--	39,138/-	1,18,914/-	-36,414/-		
8.	Total	12,97,978/-	8,41,615/-	84,847/-	3,70,272	12,96,734/-	1,244/-		

Name and Signature of Principal Investigator: (Ms. GANGUTRI SAIKIA)
Date: 15.02.2022

Signature of Competent financial authority: _____
(with seal) _____
Finance Officer _____
Date: _____

Tezpur University